ANNUAL REVIEWS **Further**

Click here for quick links to Annual Reviews content online, including:

- Other articles in this volume
- Top cited articles
- Top downloaded articles
- Our comprehensive search

Annu. Rev. Biophys. 2009.38:301-326. Downloaded from arjournals.annualreviews.org
by University of California - Berkeley on 04/07/10. For personal use only.

Particle-Tracking Microrheology of Living Cells: Principles and Applications

Denis Wirtz

Department of Chemical and Biomolecular Engineering and Institute for NanoBioTechnology, Johns Hopkins University, Baltimore, Maryland 21218; email: wirtz@jhu.edu

Annu. Rev. Biophys. 2009. 38:301–26

The *Annual Review of Biophysics* is online at biophys.annualreviews.org

This article's doi: 10.1146/annurev.biophys.050708.133724

Copyright © 2009 by Annual Reviews. All rights reserved

1936-122X/09/0609-0301$20.00

Key Words

cell mechanics, nanorheology, viscosity, elasticity, LINC complex, laminopathies, emerin

Abstract

A multitude of cellular and subcellular processes depend critically on the mechanical deformability of the cytoplasm. We have recently introduced the method of particle-tracking microrheology, which measures the viscoelastic properties of the cytoplasm locally and with high spatiotemporal resolution. Here we establish the basic principles of particle-tracking microrheology, describing the advantages of this approach over more conventional approaches to cell mechanics. We present basic concepts of molecular mechanics and polymer physics relevant to the microrheological response of cells. Particle-tracking microrheology can probe the mechanical properties of live cells in experimentally difficult, yet more physiological, environments, including cells embedded inside a 3D matrix, adherent cells subjected to shear flows, and cells inside a developing embryo. Particle-tracking microrheology can readily reveal the lost ability of diseased cells to resist shear forces.

Annu. Rev. Biophys. 2009.38:301-326. Downloaded from arjournals.annualreviews.org
by University of California - Berkeley on 04/07/10. For personal use only.

Contents

INTRODUCTION 302
BASIC CONCEPTS OF MOLECULAR CELL MECHANICS 305
Working Definitions of Stress, Viscosity, Elasticity, and Compliance 305
A Model System: A Solution of Actin Filaments 306
BASIC PRINCIPLES OF PARTICLE-TRACKING MICRORHEOLOGY 308
Particle-Tracking Microrheology of a Viscous Liquid 308
Particle-Tracking Microrheology of an Elastic Solid 312
Particle-Tracking Microrheology of a Viscoelastic Material 313
Dynamic Viscosity Versus Shear Viscosity 314
Creep Compliance from Particle-Tracking Measurements 314
PARTICLE-TRACKING MICRORHEOLOGY OF CELLS . 315
Interstitial Viscosity Versus Mesoscale Viscoelasticity of the Cytoplasm 315
Active Versus Passive Microrheology 316
Advantages of Particle-Tracking Microrheology Over Current Methods 317
Illustrative Example of Particle-Tracking Microrheology of Living Cells 319

INTRODUCTION

Many cellular and subcellular processes depend critically on the mechanical deformability of the cytoplasm. For example, the translocation of organelles (e.g., nucleus, mitochondria, and endoplasmic reticulum) within the cytoplasm is partly controlled by their frictional drag and therefore by the local viscoelastic properties of the cytoplasm (54, 55, 59, 68). Migrating cells at the edge of a wound significantly increase the stiffness of their cytoplasm to enable dendritic filamentous actin (F-actin) assemblies to produce net protruding forces against the plasma membrane (50, 80). Axonal elongation depends directly on the highly regulated intracellular viscosity of the growth cone (72). Cells need to adapt their intracellular physical properties to the physical properties of their extracellular milieu to grow, differentiate, and migrate (20, 22, 78). Moreover, changes in the mechanical properties of cells often correlate with disease state (14, 34, 58). For instance, cells derived from mouse models of progeria (premature aging) or muscular dystrophy display significantly softer (i.e., less elastic) cytoplasm (55) than wild-type controls. This affects the ability of these cells to resist shear forces and to migrate to the edge of a wound (60).

We have recently introduced the method of particle-tracking microrheology (102) to measure the viscoelastic properties of the cytoplasm locally and with high spatiotemporal resolution. In this approach, fluorescent beads of less than 1 μm in diameter are injected directly into the cytoplasm of live cells (**Figure 1**). These beads rapidly disperse throughout the cytoplasm and are subsequently tracked by fluorescence microscopy (102). The recorded movements of the beads are analyzed in terms of viscosity and elasticity of the cytoplasm. We and others have exploited particle-tracking microrheology to probe the viscoelastic properties of various types of cells in a wide range of conditions (12, 37, 45, 57, 60, 61, 67, 73, 77, 85, 92, 95, 103). These measurements have revealed important new mechanistic insights into how the physical properties of the cytoplasm adapt to various chemical and physical stimuli, how they can control basic cell functions, and how these properties can be significantly altered in diseased cells. Below, we briefly describe different cell biological questions, which have been recently addressed using particle-tracking microrheology.

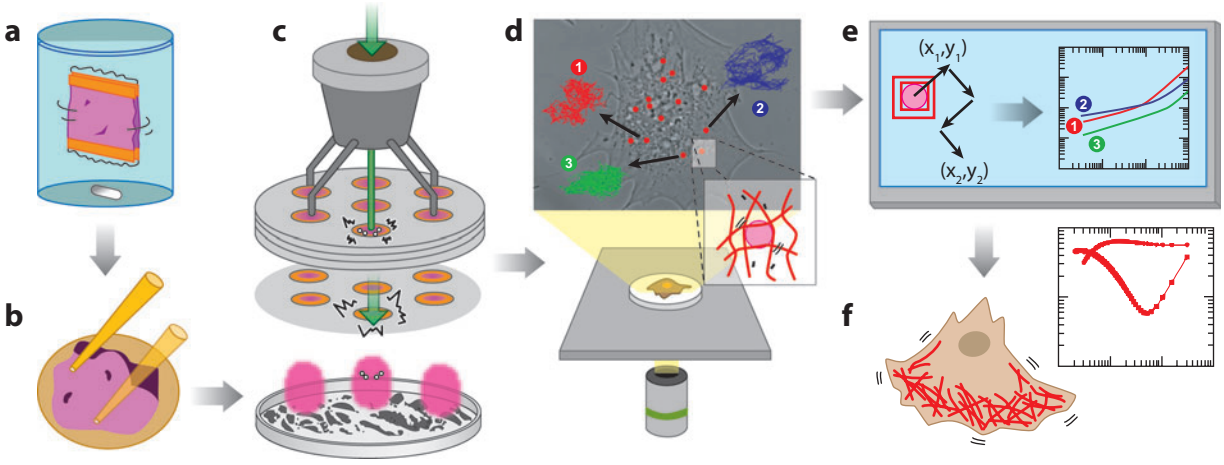

Figure 1

Particle-tracking microrheology. (*a*) Submicron fluorescent beads are dialyzed. (*b*, *c*) These beads are spread on a grid, which is placed inside a ballistic injection machine. After ballistic injection, the beads disperse rapidly within the cytoplasm. (*d*) The cells are placed under a high-magnification fluorescence microscope. The random spontaneous movements of the beads are monitored with high spatial and temporal resolution. The numerals 1, 2, and 3 refer to the order of steps in which particle-tracking is conducted. (*e*) Using the appropriate software, the time-dependent (x, y) coordinates of the beads are mathematically transformed into mean squared displacements (MSDs). (*f*) The time lag-dependent MSDs of the beads are subsequently transformed into local values of either the frequency-dependent viscoelastic moduli, $G'(\omega)$ and $G''(\omega)$, or the creep compliance, $\Gamma(t)$, of the cytoplasm. Modified with permission from Reference 76.

Annu. Rev. Biophys. 2009.38:301-326. Downloaded from arjournals.annualreviews.org
by University of California - Berkeley on 04/07/10. For personal use only.

Particle-tracking microrheology (also called nanorheology) shows that the cytoplasm of adherent cells at rest, such as endothelial cells and fibroblasts on planar substrates, is typically more elastic than viscous (i.e., these cells show a rheological behavior which is akin to that of a solid) for timescales between 0.1 and ~10 s (102). However, at timescales greater than 10–20 s, these cells show a predominantly viscous response to shear forces: The cytoplasm behaves like a liquid (102). In general, the viscoelastic properties of adherent cells are dominated by the actin filament cytoskeleton. Indeed pharmacological treatment inducing the disassembly of actin filaments eliminates the deformability of the cytoplasm and renders the cytoplasm mostly viscous at all timescales (107, 116). Moreover, the level of elasticity in the cell correlates with the local concentration of F-actin present in the cytoplasm: The actin-rich cell periphery (i.e., the lamella) is significantly stiffer than the perinuclear region, which contains less actin. Serum-starved cells, which show little organized F-actin, have both a low viscosity and a low elasticity. However, when suddenly subjected to a shear flow similar to that present in blood vessels, the cytoplasm of serum-starved cells displays rapid assembly of actin filaments into organized structures (61, 76). Particle-tracking microrheology reveals that flow-induced actin filament assembly is accompanied by a rapid rise in cytoplasmic stiffness, followed by an equally rapid decrease in stiffness (61). This transient increase in cytoplasmic stiffness correlates with the transient activation of the Rho/Rho kinase (ROCK) pathway and the associated assembly and transient contraction of the actin filament network by myosin II. These results suggest that when an adherent cell is subjected to shear stresses, its first action is to prevent detachment from its substratum by greatly stiffening the cytoplasm through enhanced actin filament assembly and Rho-kinase-mediated contractility.

During migration at the edge of a wound, cells polarize their overall morphology and

Annu. Rev. Biophys. 2009.38:301-326. Downloaded from arjournals.annualreviews.org
by University of California - Berkeley on 04/07/10. For personal use only.

position the microtubule organizing center (MTOC) toward the cell's leading edge (31, 59). Particle-tracking microrheology indicates that the mechanical properties of the cytoplasm become spatially polarized as well: The cytoplasm is much stiffer at the leading edge than at the trailing edge of the migrating cell, i.e., the region near the nucleus that is positioned near the back of the cell (50). MTOC repositioning at the edge of the wound is abrogated in cells transfected with a dominant-negative mutant of the small GTPase Cdc42 (98). Similarly, cells with deactivated Cdc42 show no spatial polarization in their mechanical properties. These results suggest that a differential distribution of subcellular mechanical microenvironments is essential for directed cell migration and is coordinated through microtubules (50).

Particle-tracking microrheology has also shown that the elasticity of the cytoplasm is much lower than that of the nucleus in the same cell. The nucleus is also more elastic than viscous, which reveals that the intranuclear region displays an unexpectedly strong solid-like behavior (103). Indeed, when cells move though a dense extracellular matrix, a rate-limiting step in the 3D migration process is the squeezing of the nucleus by the pores of the matrix, not the deformation of the cytoplasm (6, 56). Measurements of the mean shear viscosity and the elasticity of the intranuclear region determine a lower bound of the propulsive forces (3–15 pN) required for nuclear organelles such as the promyelocytic leukemia body to undergo processive transport within the nucleus by overcoming the friction forces set by the intranuclear viscosity. Dynamic analysis of the spontaneous movements of submicron beads embedded in the nucleus also reveals the presence of transient nuclear microdomains of mean size 290 nm that are mostly absent in the cytoplasm (32, 103). The strong elastic character and the micro-organization of the intranuclear region revealed by particle-tracking analysis may help the nucleus preserve its structural coherence. This study highlights the difference between the low interstitial nucleoplasmic viscosity, which controls the transport of nuclear proteins and molecules, and the much higher mesoscale viscosity, which affects the diffusion and the directed transport of nuclear organelles and reorganization of interphase chromosomes (103).

Finally, particle-tracking microrheology has shown that when human endothelial cells are placed inside a 3D matrix, their cytoplasm is much softer than when the same cells are placed on a thin planar layer of the same matrix (77). Vascular endothelial growth factor (VEGF) treatment, which enhances endothelial migration in the 3D matrix, increases the deformability of the cytoplasm of endothelial cells in the matrix. This VEGF-induced softening response of the cytoplasm is abrogated by specific ROCK inhibition. These results suggest that ROCK plays an essential role in the regulation of the intracellular mechanical response to VEGF of endothelial cells in a 3D matrix.

The above measurements could only have been achieved thanks to particle-tracking microrheology, which can reveal the mechanical properties of live cells in experimentally difficult—yet more physiological—environments. For instance, particle-tracking microrheology is the only cell mechanics method that can probe the mechanical properties of individual cells deeply embedded inside a 3D matrix and their mechanical response to agonists and/or drug treatments (77), monitor changes in cytoskeleton elasticity in cells subjected to shear flows (61), or measure in vivo the local viscoelastic properties of a *Caenorhabditis elegans* embryo embedded in an impenetrable shell (16). Cells in these more physiological environments cannot be probed by existing methods of cell mechanics, such as atomic force microscopy (AFM), because these cells are inaccessible to direct physical contact and can only be probed at a distance.

This review describes basic concepts of molecular mechanics and polymer physics applied to cells and introduces the fundamental principles underlying particle-tracking microrheology and its advantages over traditional cell mechanics methods. This review also shows how particle-tracking microrheology can

readily reveal the lost ability of diseased cells to resist shear forces.

BASIC CONCEPTS OF MOLECULAR CELL MECHANICS

Working Definitions of Stress, Viscosity, Elasticity, and Compliance

Because different experimental methods measure different (but often related) rheological quantities, the intracellular mechanics of a living cell is best characterized by multiple rheological parameters, including viscosity, elasticity, and creep compliance. These rheological parameters simply describe the mechanical response of a material (such as the cell's cytoplasm) subjected to a force and how it measures the resulting deformation and, vice versa, the mechanical response of a material subjected to a deformation and how it measures the force required to produce the deformation. The rheological response of the cytoplasm can be either predominantly viscous or elastic, depending on the time of application and the magnitude of the force. These forces can be externally applied as in the case of endothelial cells subjected to blood flow (61), result from internal tension as in the case of actomyosin contractility, or both (49).

The shear viscosity of a liquid measures its propensity to flow under random or applied forces. The shear viscosity generates the drag forces that slow down the motion of organelles and protein complexes in the cytoplasm and nucleus. A simple way to measure the viscosity of a material or liquid is to use a falling-ball viscometer. Here the speed at which heavy metallic beads fall through the probed material depends on an effective viscosity. This method is highly approximate due to the uncontrolled interactions between the beads and the material, the inherent difficulty to measure the terminal velocity of the beads, and the assumptions that need to be made to compute this viscosity. Alternatively, the material can be subjected to a steady shear deformation of controlled rate using a rheometer. Here, the material is placed between two parallel plates or between a cone and plate. The viscosity is the ratio of the stress (force per unit area) induced in the material by the imposed deformation to the rate of shear deformation. In cells, the viscosity of the cytoplasm predominantly governs the transport and movements of subcellular organelles and cytoskeleton structures at long timescales. A material that is only viscous (and not elastic), such as water, cannot resist mechanical stresses; it can only slow down its deformation by the imposed mechanical stress. Upon cessation of the stress, the material or liquid has lost all memory of its original shape and location. Below, we show how the viscosity of a material or a liquid can be obtained by tracking the random movements of submicron beads embedded in the material.

The elasticity (also called the elastic modulus) of a material measures its stretchiness. Elasticity measures the ability of cytoplasmic structures to resist forces and store energy caused by deformation. A material that is only elastic (and not viscous) can deform under stress but cannot flow. As no viscous dissipation occurs during its deformation, the elastic material snaps back to its original shape upon cessation of the stress. Elasticity typically governs the response of the cytoplasm to mechanical stresses at short timescales.

Some materials, such as Silly Putty®, can be both viscous and elastic. Silly Putty can bounce as it deforms upon impact, but quickly regains its shape, which means it is elastic. It is also viscous, as Silly Putty rolled into a ball will partially flatten due to its own weight when left on a flat surface. These simple observations indicate that Silly Putty is elastic at short timescales (i.e., during impact) and viscous at long timescales. Similarly, the cytoplasm of living cells is both viscous and elastic, i.e., it is viscoelastic.

Instead of working in the time domain, rheologists tend to work in the frequency domain. The frequency-dependent elastic modulus of a material, $G'(\omega)$, can be obtained by subjecting it to oscillatory deformations of controlled frequency ω and constant (small) amplitude. When an oscillatory deformation is applied and is given by a sine function of time,

Annu. Rev. Biophys. 2009.38:301-326. Downloaded from arjournals.annualreviews.org
by University of California - Berkeley on 04/07/10. For personal use only.

Annu. Rev. Biophys. 2009.38:301-326. Downloaded from arjournals.annualreviews.org
by University of California - Berkeley on 04/07/10. For personal use only.

$\gamma(t) = \gamma_0 \sin \omega t$, the stress, τ, induced within the material by this deformation will typically have both sine and cosine components. Specifically, the stress can be decomposed into a sine (in-phase) component and a cosine (out-of-phase) component: $\tau(t) = \tau' \sin \omega t + \tau'' \cos \omega t = \gamma_0(G' \sin \omega t + G'' \cos \omega t)$. The elastic modulus of the material, G', is equal to the in-phase component of the frequency-dependent stress divided by the amplitude of the oscillatory deformation, i.e., $G'(\omega) = \tau'/\gamma_0$. The viscous modulus of the same material, $G''(\omega)$, can be obtained during the same measurement by extracting the out-of-phase component of the frequency-dependent stress and dividing by the amplitude of the oscillatory deformation, i.e., $G''(\omega) = \tau''/\gamma_0$ (24). If the material is an elastic solid (no or little viscosity), such as rubber, then the induced stress is exactly in phase with the input deformation and $\tau(t) = \tau' \sin \omega t$. In this case, $G'' = 0$. If the material is a viscous liquid (no elasticity), such as water or glycerol, then the induced stress is out of phase with the input deformation, and $\tau(t) = \tau'' \cos \omega t$. In this case, $G' = 0$.

Typical biological materials, such as cells and tissues, have rheological properties that depend on the rate of deformation, ω, i.e., both G' and G'' depend on ω. At low frequencies, the cytoplasm has the time to reorganize its cytoskeleton polymers and it can flow, behaving as a viscous liquid. At high frequencies, the cytoplasm does not have the time to reorganize and the cytoplasm behaves as an elastic solid, which resists the deformation. This underlies the importance of measuring the full frequency-dependent response of cells and tissues, which undergo both slow and rapid movements. However, the rheology of individual cells cannot be measured with a macroscopic device, such as a rheometer. Moreover, even if a microscopic rheometer existed, measuring the full frequency-dependent rheological response of the cytoplasm to oscillatory deformations would be tedious, as this response would have to be probed one frequency at a time over a wide range of frequencies. Below, we show that the frequency-dependent viscous and elastic moduli of a cell can be obtained in ~10 s from the dynamic movements of submicron probe beads embedded in the cytoplasm, without subjecting the cell to any external force or deformation.

A material that is only viscous and has no elasticity, such as water, is a liquid and $G' = 0$. A material that is only elastic and has no or little viscosity, such as rubber or Jell-O, is a solid and $G'' \approx 0$. A material that is more viscous than elastic, i.e., $G''(\omega) > G'(\omega)$, is a viscoelastic liquid; a material that is more elastic than viscous, $G'(\omega) > G''(\omega)$, is a viscoelastic solid.

Finally, the creep compliance of the cytoplasm refers to its deformability. Experimentally, it is measured by the deformation of the cytoplasm resulting from an applied mechanical stress (applied force). A high compliance indicates that a material has a low propensity to resist mechanical deformation following application of a shear stress; a low compliance indicates that it can resist such stress. When the material is only viscous or only elastic and not both, the creep compliance of the material is inversely proportional to its viscosity or elasticity, respectively. Below, we show how the time-dependent creep compliance of the cytoplasm can be obtained directly from tracking the movements of submicron probe beads embedded in the cytoplasm, without subjecting the cell to any external force.

Viscoelastic moduli (G' and G'') and creep compliance of the cytoplasm are related. Indeed, it is possible to compute the time-dependent cytoplasmic creep compliance from the frequency-dependent viscoelastic parameters and, vice versa, the viscoelastic moduli of the cytoplasm can be computed from the time-dependent creep compliance. The shear viscosity can also be estimated from the frequency-dependent viscous and elastic moduli.

A Model System: A Solution of Actin Filaments

To obtain a more intuitive understanding of the rheological concepts defined above, we consider the simple (but not trivial) system of a concentrated solution of actin filaments. A

key contributor to cytoplasmic stiffness is the cytoskeleton, which is composed of three major filamentous proteins: F-actin, microtubules, and intermediate filaments (92). The cytoskeleton provides the cytoplasm with its structure and shape. In the cell, actin monomers assemble into semiflexible F-actin polymers that readily form entangled networks (30, 97, 108) whose viscoelastic properties can be controlled by either altering the local density of actin filaments or the cross-linking/bundling activity of F-actin-binding proteins, such as α-actinin or filamin (43, 113). In most cells, F-actin and intermediate filaments are the primary contributors to cytoplasmic stiffness (92).

The cytoplasm of adherent cells is rheologically complex: It typically behaves as a viscoelastic liquid when sheared either slowly or for a long time, and as a viscoelastic solid when sheared either rapidly or for a short time. This rheological complexity can be captured by a solution of entangled actin filaments in vitro in the absence of motor or cross-linking proteins (3, 47). Below a threshold concentration of ~0.2 mg/ml, actin filaments cannot resist shear deformations; their global rheological response is viscous, with a viscosity equal to that of buffer, with a small additional correction due to the presence of the filaments (17). However, past this threshold concentration, the actin filaments in suspension begin to form entanglements. Because these filaments are rigid (30), they form entanglements more readily than flexible polymers that have the same contour length. These entanglements form topological obstacles in the network that impede the lateral bending motion of the filaments, but not their longitudinal movements. These polymer entanglements render the solution of actin filaments elastic.

At short timescales, the filaments only undergo thermally driven lateral fluctuations

Annu. Rev. Biophys. 2009.38:301-326. Downloaded from arjournals.annualreviews.org
by University of California - Berkeley on 04/07/10. For personal use only.

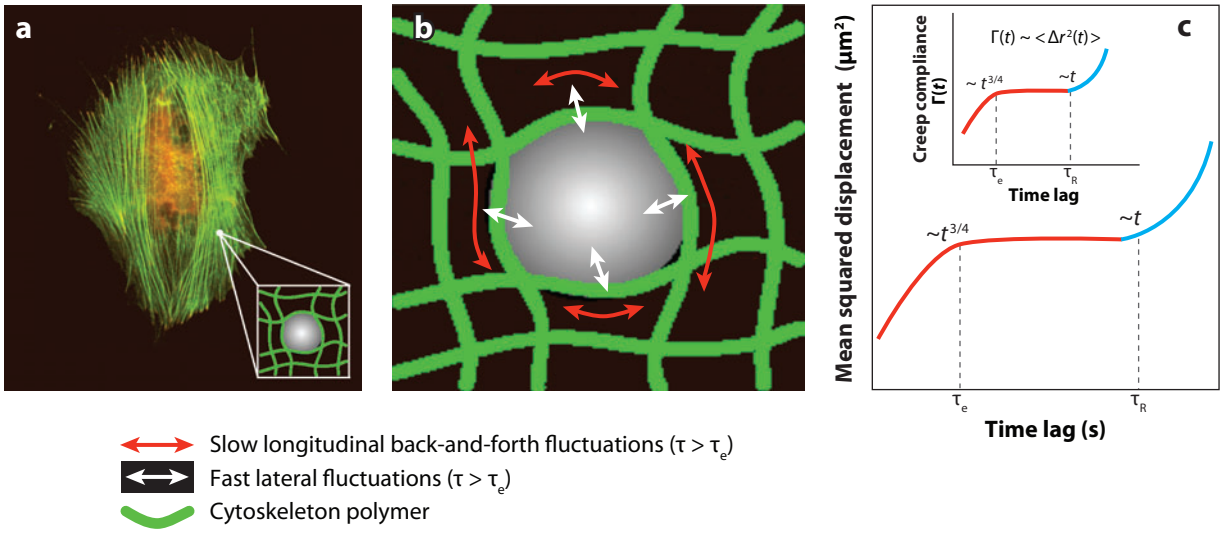

Figure 2

Physical origin of the displacements of beads in the cytoplasm. (*a*) Ballistically injected beads are lodged within the cytoskeleton. The size of the beads is larger than the average mesh size of the cytoskeleton network, which is ~50 nm in fibroblasts. (*b*) The spontaneous movements of the cytoskeleton filaments that surround each bead induce displacements of the beads. At short timescales, the displacements of the beads are predominantly induced by the fast lateral bending fluctuations of the cytoskeleton filaments. At long times, the displacements of the beads are predominantly induced by the slow longitudinal back-and-forth lateral fluctuations of the cytoskeleton filaments. Finally, filaments move sufficiently to allow beads to escape the cage to move to the next cage. (*c*) Accordingly, the mean squared displacements (MSDs) of the beads show a $t^{3/4}$ power-law dependence at short timescales, a quasi plateau value at intermediate timescales between τ_e and τ_R, and a linear dependence at long times caused by the slow viscous diffusion of the beads. (*Inset*) The deformability of the cytoplasm [creep compliance, $\Gamma(t)$] is proportional to the MSD of the beads, $\langle \Delta r^2(t) \rangle$. See text for details.

Annu. Rev. Biophys. 2009.38:301-326. Downloaded from arjournals.annualreviews.org
by University of California - Berkeley on 04/07/10. For personal use only.

(**Figure 2**). These fluctuations are fast, as they involve small sections of the filaments between network entanglements. A fast camera shows each actin filament undergoing lateral fluctuations within a confining tube-like region formed by the surrounding filaments (17, 18, 46). At intermediate timescales that are longer than the time for the lateral fluctuations to begin to hit the walls of the tube region, the back-and-forth longitudinal movements of the filament in the network can take place (**Figure 2**). These longitudinal motions are slow because they involve the entire filament. But these back-and-forth movements result in no net displacement of the filaments: The movements of the filaments are effectively curved 1D random walks. Finally, at timescales longer than a characteristic terminal relaxation time of the network, which depends on the length of the filament, the filament can finally escape the tube-like region (39, 70).

This description of the timescale-dependent movements of individual filaments in a dense network can be redescribed in rheological terms for the whole filament network following de Gennes' original concept (17). Consider an actin filament network subjected to a constant stress (force per unit area) of relatively small magnitude. At short timescales, the filaments can only relax the energetically unfavorable distortions, which are created in the polymer network by the externally applied stress, through lateral fluctuations (70). The creep compliance—or the deformation of the network—increases as a function of time as $t^{3/4}$ (114) (**Figure 2*c***). The exponent 3/4 reflects the lateral bending fluctuations of the filaments (70, 74). At longer timescales, the network cannot relax anymore because no net filament motion occurs at these timescales. Accordingly, the creep compliance of the filament network becomes approximately constant (or a quasi plateau, **Figure 2*c***) and the network behaves mostly as an elastic gel, as the elastic modulus becomes much larger than the viscous modulus. A stably cross-linked actin filament network behaves similarly, but at all timescales (44). At long timescales, the filaments can finally diffuse out of their confining tubes, the network can relax the stress, and the creep compliance grows linearly with time, a proportionality that reflects viscous diffusion (21). The network becomes a viscoelastic liquid, for which the viscous modulus is much larger than the elastic modulus (24). If the actin filament network is stably cross-linked, the polymer cannot undergo this terminal relaxation and the plateau value of the compliance persists indefinitely. Often the transition from the plateau region to the terminal relaxation is not sharp because actin filaments have a wide distribution of lengths, which define a broad distribution of relaxation times.

A permanently cross-linked actin filament network provides cells with structural stability but does not allow them to readily soften to allow for cell shape changes that are, for instance, required during intravasation and extravasation of cancer cells in and out of blood vessels (110). To circumvent this problem and allow for a stiff but malleable cytoskeleton, cells have evolved an ingenious mechanism. This mechanism does not require dynamic disassembly and reassembly of the filaments themselves to modulate the mechanical properties of the network. Instead F-actin networks exploit dynamic cross-linking proteins, such as filamin or α-actinin (25, 99, 109, 110). When such a network is sheared more slowly than the lifetime of binding of the cross-linking protein, the network can flow and behaves mostly as a liquid. When sheared at a rate faster than the inverse binding lifetime of the cross-linking protein, the actin filament network behaves as an elastic gel and cannot flow (109, 110, 115).

BASIC PRINCIPLES OF PARTICLE-TRACKING MICRORHEOLOGY

Particle-Tracking Microrheology of a Viscous Liquid

To understand how the viscoelastic properties of the cytoplasm of cells can be obtained by tracking the movements of beads embedded in it, we consider first the simpler limit case of

Annu. Rev. Biophys. 2009.38:301-326. Downloaded from arjournals.annualreviews.org
by University of California - Berkeley on 04/07/10. For personal use only.

submicron beads suspended in a viscous liquid (no elasticity). These beads are smaller than 1 μm so that they undergo Brownian motion, as inertial forces (gravity) are negligible. If active transport of the nanoparticles is also negligible, only two types of forces act on the beads inside the cytoplasm:

- The small random force produced by the random bombardment of water molecules generated by the thermal energy k_BT and the movements of other cytoplasmic structures, such as cytoskeleton filaments and other organelles (102).
- The counteracting frictional force, which results from the movement of the beads driven by thermal energy. The frictional force is proportional to the velocity of the bead and the bead's friction coefficient, which depends on the viscoelastic properties of the cytoplasm and the size of the bead.

Because we neglect inertia and directed motion, the mathematical equation describing the motion of a bead simply states that the sum of these two forces is zero. This resulting equation is not deterministic, but stochastic, because the force that powers the bead movements is random in amplitude and direction. The solution of this stochastic equation, i.e., the time-dependent coordinates of the bead, is the conventional random walk (5). Therefore, on average, the bead remains at the same position. However, the standard deviation of the displacements or the mean squared displacement (MSD) of the bead, $\langle \Delta r^2 \rangle$, is not zero.

In a liquid of unknown shear viscosity, η, the submicron bead undergoes Brownian motion driven by the thermal energy k_BT. Each time the bead takes a step in a random direction, it loses all memory of where it just came from. The next step occurs in an uncorrelated direction. Einstein showed that, in these conditions, the bead undergoes a random walk and its time-averaged MSD is simply $\langle \Delta r^2 \rangle = 4Dt$ (**Figure 3*a***). Here t is time lag, $\langle ... \rangle$ indicates time-averaging, and D is the diffusion coefficient of the bead. The linear dependence of the MSD on time lag is a signature of pure viscous diffusion of the bead (81). Equivalently, the square-root dependence of the root MSD with time, $\sqrt{\langle \Delta r^2 \rangle} = \sqrt{4Dt} \sim t^{1/2}$, is a signature of viscous diffusion (5). For a spherical bead, the diffusion coefficient is given by the relation $D = k_BT/\xi$ (Stokes-Einstein relation), where $\xi = 6\pi\eta a$ is the friction coefficient of the bead in the liquid and a is the radius of the bead. After rearrangements, one finds that the

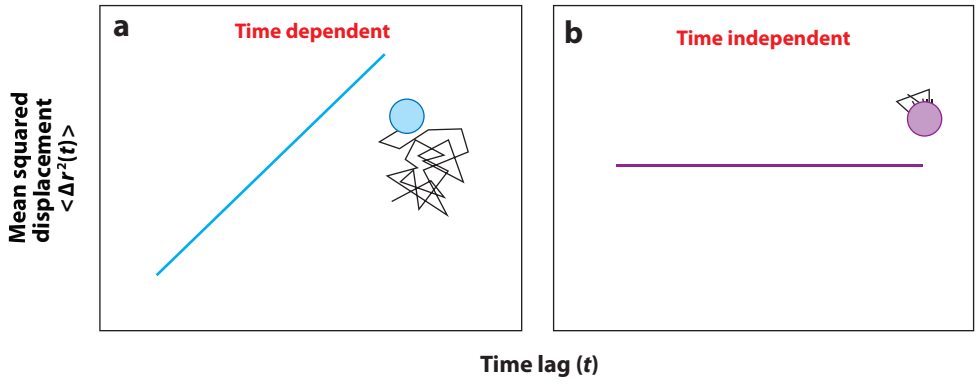

Figure 3

Particle-tracking microrheology of a viscous liquid and an elastic solid. (*a*) The mean squared displacement (MSD) of beads immersed in a viscous liquid (such as water or glycerol) grows linearly with time lag, with a slope inversely proportional to the viscosity of the liquid and the radius of the bead. (*b*) The MSD of beads embedded in an elastic solid (such as rubber) is independent of time lag. The plateau value is inversely proportional to the elasticity of the solid.

viscosity of the liquid can be estimated as soon as the MSD of the bead is measured (114):

$$\eta = \frac{2k_BT}{3\pi a}\frac{t}{\langle \Delta r^2(t)\rangle}. \qquad 1.$$

This expression explains how one can estimate the viscosity of a liquid merely by suspending small beads in that liquid, subsequently tracking their thermally excited random motion using fluorescence light microscopy and appropriate particle-tracking software, and finally computing the MSD from the trajectories of the beads.

In practice, tens to hundreds of beads need to be tracked to ensure adequate statistical averaging. In this case, the ensemble-averaged MSD, $\langle\langle \Delta r^2(t)\rangle\rangle$, which is the means of all measured MSDs, is used instead of $\langle \Delta r^2\rangle$. If the suspending fluid is indeed a liquid, then $t/\langle \Delta r^2(t)\rangle$ should be a constant independent of t (see Equation 1), which is a stringent test of viscous diffusion. If $t/\langle \Delta r^2(t)\rangle$ is nonconstant, it usually indicates that the suspending fluid is a viscoelastic material instead of a viscous liquid (65).

We consider a 100-nm-diameter bead suspended in corn syrup, which has a shear viscosity close to that of the cytoplasm of fibroblasts, $\eta = 20$ P $= 2$ Pa.s (typical values of viscosity are listed in **Table 1**). The thermal energy is $k_BT \approx 4.2$ pN.nm (where $T = 37°$C) and the diffusion coefficient of the bead is $D \approx 0.0022$ μm^2/s. By comparison, the diffusion of the same bead in water is 4.4 μm^2/s. Therefore, the value of the time-averaged MSD of the bead after $t = 0.1$ s, 1 s, and 10 s of tracking is $\approx$0.00088 μm^2 (or 88 nm^2), 0.0088 μm^2, and 0.088 μm^2, respectively. This result indicates that the average size of the region crisscrossed by the Brownian movements of the bead after the same times is $\sqrt{\langle \Delta r^2\rangle} = \sqrt{4Dt} \approx 30$, 94, and 300 nm, respectively. This result suggests that high-resolution tracking is required to obtain good measurements of MSDs of 100-nm beads in a highly viscous liquid within a 10-s-long tracking time.

The prefactor 4 in the expression $\langle \Delta r^2\rangle = 4Dt$ stems from the fact that microscopy probes the 2D projection of an intrinsically 3D movement of the bead. This is correct only if the material in the proximity of the bead is isotropic, i.e., this material or liquid has the same physical properties in all three (x, y, and z) directions. To test whether this is likely to be true without tracking the movements of the beads in all three directions (19), one can compute the MSDs of the bead in the x and y directions independently. Indeed, from the measured time-dependent coordinates of the bead, $x(t)$ and $y(t)$, the MSD is given by $\langle \Delta r^2(t)\rangle = \langle [x(t) - x(0)]^2 + [y(t) - y(0)]^2\rangle$, where $x(0)$ and $y(0)$ correspond to the initial position of the bead. If the material is isotropic, then $\langle [x(t) - x(0)]^2\rangle = \langle [y(t) - y(0)]^2\rangle$ and therefore $\langle \Delta r^2(t)\rangle = 2\langle [x(t) - x(0)]^2\rangle = 2\langle [y(t) - y(0)]^2\rangle$. If the MSDs of the bead in the x and y directions are indeed Brownian (corresponding to two independent 1D random walks), then $\langle [x(t) - x(0)]^2\rangle = \langle [y(t) - y(0)]^2\rangle = 2Dt$. Hence, $\langle \Delta r^2(t)\rangle = 4Dt$, and therefore it is likely that the MSDs of the bead in the z direction are also Brownian and equal to those in the x and y directions, which indicates that the viscoelastic properties of the cytoplasm in the vicinity of the bead are isotropic (38).

In the case of a viscous liquid, the elastic modulus of the liquid is of course zero, $G' = 0$, and it can be shown that the viscous modulus is simply $G'' = \eta\omega$. Here ω is the frequency (or rate) of deformation in an oscillatory mode of deformation and is equal to the inverse of the time lag t, $\omega = 1/t$. This means that if this liquid were placed in a rheometer and subjected to oscillatory deformations, then the elastic modulus would be negligible and the viscous modulus would increase linearly with the input frequency ω. Equivalent to the linear dependence of the MSD with time, that the viscous modulus of a given material increases linearly with the rate of deformation indicates that this material is a viscous liquid. This rheological response, i.e., $G' \approx 0$ and $G'' = \eta\omega$, is for instance that of an unpolymerized G-actin solution in vitro or that of the cytoplasm of a cell treated with an actin-depolymerizing drug (e.g., latrunculin A or cytochalasin D).

Annu. Rev. Biophys. 2009.38:301-326. Downloaded from arjournals.annualreviews.org
by University of California - Berkeley on 04/07/10. For personal use only.

Table 1 Elasticity and shear viscosity of the cytoplasm of different types of cells measured by particle-tracking microrheology[a]

Cell type and condition; values of viscoelastic parameters	Average viscosity (poise)	Average elasticity at 1 Hz (dyne/cm^2)	Reference
Serum-starved Swiss3T3 fibroblast[b]	10 ± 3	50 ± 20	(49)
Serum-starved Swiss 3T3 fibroblast treated with LPA[c]	95 ± 20	120 ± 30	(49)
Serum-starved Swiss3T3 fibroblast subjected to shear flow[d]	300 ± 40	600 ± 50	(61)
Swiss 3T3 fibroblast at the edge of a wound[e]	45 ± 15	330 ± 30	(50)
Swiss 3T3 fibroblast treated with bradykinin[f]	22 ± 13	90 ± 20	(50)
Swiss 3T3 fibroblast treated with PDGF[g]	24 ± 8	190 ± 30	(50)
Mouse embryonic fibroblast (*Lmna*$^{+/+}$ MEF)[h]	18 ± 2	140 ± 30	(60)
MEF treated with latrunculin B[i]	NA	80 ± 4	(60)
MEF treated with nocodazole[j]	NA	50 ± 4	(60)
MEF deficient in lamin A/C (*Lmna*$^{-/-}$ MEF)	8 ± 1	60 ± 4	(60)
HUVEC on a planar 2D peptide matrix[k]	17 ± 1	130 ± 10	P. Panorchan, J.S.H. Lee, D. Wirtz, unpublished data
HUVEC on a planar 2D peptide matrix and treated with VEGF[l]	8 ± 1	100 ± 5	P. Panorchan, J.S.H. Lee, D. Wirtz, unpublished data
HUVEC inside a 3D peptide matrix[k]	14 ± 1	55 ± 4	(77)
HUVEC inside a 3D peptide matrix treated with VEGF[l]	18 ± 1	40 ± 3	(77)
HUVEC inside a 3D fibronectin matrix	NA	58 ± 6	(117)
HUVEC inside a 3D fibronectin matrix treated with inhibiting FN peptide	NA	20 ± 4	(117)
Single-cell *C. elegans* embryo[m]	10 ± 1	Negligible	(16)
Interphase nucleus of Swiss 3T3 fibroblast[n]	520 ± 50	180 ± 30	(103)

[a]Particle-tracking microrheology was used to study the mechanical properties of many varieties of cells under a wide range of conditions. Unless stated, all values of viscosity and elasticity in the table are for the cytoplasm. The elasticity was evaluated at a shear frequency of 1 s^{-1} (1 s^{-1} = 1 Hz) and the shear viscosity was estimated as the product of plateau modulus and the relaxation time. The plateau modulus is the value of the elastic modulus at intermediate frequencies where it reaches a quasi plateau value. The relaxation time is the inverse of the frequency where elastic and viscous moduli are equal. All measurements are mean ± sem. Unit conversions are 1 dyne/cm^2 = 0.1 Pa = 0.1 N/m^2 = 0.1 pN/μm^2. Pa, Pascal; pN, piconewton; NA, not available.
[b]Cells placed on 50 μg/ml fibronectin deposited on glass were serum starved for 48 h before measurements.
[c]Serum-starved cells placed on 50 μg/ml fibronectin deposited on glass were treated with 1 μg/ml lysophosphatidic acid (LPA), which activates Rho-mediated actomyosin contractility. LPA was applied 15 min before measurements.
[d]Cells were grown on 20 μg/ml fibronectin for 24 h and exposed to shear flow (wall shear stress, 9.4 dyne/cm^2) for 40 min before measurements.
[e]Cells in complete medium and grown on 50 μg/ml fibronectin to confluence were wounded to induce migration. Measurements were conducted 4 h after wounding.
[f]Cells in complete medium and grown on 50 μg/ml fibronectin were treated with 100 ng/ml bradykinin for 10 min before measurements.
[g]Cells in complete medium and grown on 50 μg/ml fibronectin were treated with 10 ng/ml platelet-derived growth factor (PDGF) for 10 min before measurements.
[h]Cells in complete medium were grown on glass.
[i]*Lmna*$^{+/+}$ mouse embryonic fibroblasts (MEFs) in complete medium grown on glass were treated with 5 μg/ml actin-filament disassembly drug latrunculin B.
[j]*Lmna*$^{+/+}$ MEFs in complete medium and grown on glass were treated with 5 μg/ml microtubule disassembly drug nocodazole.
[k]Cells in complete medium were placed in a 0.5% puramatrix gel. HUVEC, human umbilical vein endothelial cell.
[l]Cells in complete medium were placed in a 0.5% puramatrix gel and treated with 4 ng/ml vascular endothelial growth factor (VEGF) for 24 h prior to the measurements.
[m]Young *Caenorhabditis elegans* eggs were obtained by cutting gravid hermaphrodites from worms in egg salts. The nanoparticles were then microinjected into the syncytial gonads of gravid hermaphrodites.
[n]Cells in complete medium.

Annu. Rev. Biophys. 2009.38:301-326. Downloaded from arjournals.annualreviews.org
by University of California - Berkeley on 04/07/10. For personal use only.

Annu. Rev. Biophys. 2009.38:301-326. Downloaded from arjournals.annualreviews.org
by University of California - Berkeley on 04/07/10. For personal use only.

If the probed system were in equilibrium and perfectly uniform, tracking one bead for a long time (e.g., 1000 s) and dividing this time span into 100 equal time spans of 10 s should be equivalent to tracking 100 beads each for 10 s. Although it is impractical to track a single bead for a long time even in in vitro systems because of drift problems, this equivalency is correct for liquids such as water and glycerol, a signature of ergodicity. But it is incorrect in suspensions of actin filaments in vitro and in live cells, which are systems far from equilibrium and highly spatially heterogeneous (100, 104). Indeed, beads well dispersed in the cytoplasm show a wide distribution in MSDs (102).

We note that individual trajectories of the beads, even in water, are typically highly asymmetric in shape (38). Even the overall shape of a computer-generated random walk is highly asymmetric (5, 87), i.e., it is not a circle. The shape of the object encompassing an individual trajectory of a single bead in a liquid is an ellipse in the 2D space (e.g., a protein diffusing within the plasma membrane) and an ellipsoid in the 3D space (e.g., GFP diffusing in the cytoplasm) (36). However, when these trajectories are ensemble-averaged and the trajectories are superimposed, the object encompassing these individual trajectories is a circle in 2D and a sphere in 3D.

Particle-Tracking Microrheology of an Elastic Solid

The second limit example involves the same bead, but this time embedded in a highly elastic material of negligible viscosity, such as rubber. Each time the bead is driven by the thermal energy in a random direction, the surrounding material pushes back instantaneously with equal force in the opposite direction. Therefore, the MSD of the bead is finite but constant: $\langle \Delta r^2 \rangle = K$ at all timescales (**Figure 3*b***). The independence of the MSD with time is a signature of purely elastic solid behavior. The viscous modulus of this elastic solid is of course $G''(\omega) = 0$. The elastic modulus of an elastic solid is simply $G'(\omega) = 2k_BT/3\pi a\langle \Delta r^2 \rangle = 2k_BT/3\pi aK$, which is a constant independent of ω, i.e., the elastic modulus of an elastic solid is inversely proportional to the MSD of the beads embedded in it. This expression shows that one can compute the elastic modulus of an elastic solid from particle-tracking measurements of $\langle \Delta r^2 \rangle$ without imposing any oscillatory deformation. The fact that the elastic modulus of a given material is independent of the rate of deformation or frequency, ω, is a signature of purely elastic behavior. This would be the rheological response of a permanently cross-linked actin filament network (75) or Jell-O, where G' is approximately a constant independent of frequency and G'' is much smaller than G'.

Let us consider a 100-nm-diameter bead suspended in a stiff elastic material of frequency-independent elasticity of $G' = 10\ \text{Pa} = 100\ \text{dyne/cm}^2$. Typical values of elasticity are given in **Table 1**. Then, the time-averaged MSD of the bead in this material at all timescales is $\langle \Delta r^2 \rangle = 2k_BT/3\pi aG' \approx 0.002\ \mu\text{m}^2$, which can readily be measured by fluorescence microscopy and appropriate particle-tracking software.

These two examples—viscous liquid and elastic solid—illustrate how the time dependence of the MSD of beads inside a given material can help rapidly diagnose key physical properties of the material, including whether it is a liquid (then, $\langle \Delta r^2 \rangle \sim t$ or $\langle \Delta r^2 \rangle / t$ is a constant) or an elastic solid (then, $\langle \Delta r^2 \rangle$ is a constant).

The results above indicate that to estimate the viscosity of a liquid, a spatial resolution of at least 30 nm is required when tracking 100-nm-diameter beads for 10 s using a camera that collects images at a rate of 10 frames per second. In practice, the spatial resolution on the displacements of the beads must be an order of magnitude better, approximately 3 nm for a 100-nm-diameter fluorescent bead. Such a high, subpixel spatial resolution can be obtained by using either quadrant detection or fluorescence video microscopy. The advantage of quadrant detection is its superior detection capability (<1 nm) (93), but quadrant detection can only track one or two beads at a time (28, 29, 116). This is a serious problem when it is

desirable to monitor simultaneously the viscoelastic properties of various locations within the cell. When using high-magnification, high-numerical-aperture lenses (11), video microscopy allows one to track hundreds of beads at the same time (13, 86, 102) but has a maximum resolution of the order of 3–10 nm, depending on the experimental setup. The spatial resolution of the measurements will vary from one instrument to another as it also depends on the stability of the microscope system used to track the beads. For a material that is essentially elastic and with a maximum spatial resolution of 3 nm, the highest elasticity that can still be measured with accuracy using particle-tracking microrheology is approximately $G'_{max} = 2k_B T/3\pi a(3\,\text{nm})^2 \approx 1{,}900\,\text{Pa} \approx 19{,}000\,\text{dyne/cm}^2$ (88, 89), which is much higher than typical values of the elasticity of the cytoplasm. Therefore, using video microscopy and high-resolution tracking allows for the measurements of highly elastic materials.

Particle-Tracking Microrheology of a Viscoelastic Material

The rheological behavior of the cytoplasm or a reconstituted actin filament network is intermediate between the two limit behaviors of a viscous liquid and an elastic solid, as described above. Indeed, the cytoplasm is predominantly viscous at long timescales ($t > \tau_R$) or low rates of shear, $G''(\omega) \gg G'(\omega)$ for $\omega < \omega_R$, and predominantly elastic at short timescales or high rates of shear, $G''(\omega) \ll G'(\omega)$ for $\omega > \omega_R$, where ω_R is the inverse of the relaxation time of the cytoskeleton network, τ_R (**Figure 4**). At high frequencies, $\omega > \omega_e$, both G' and G'' are proportional to $\omega^{3/4}$, a power-law dependence that reflects the bending lateral fluctuations of the semiflexible filaments in the network (40, 90). The exponent would be 1/2 if the polymers constituting the cytoskeleton were flexible (21), but intermediate filaments, actin filaments, and microtubules in live cells are semiflexible (1). The frequency ω_e is approximately equal to the

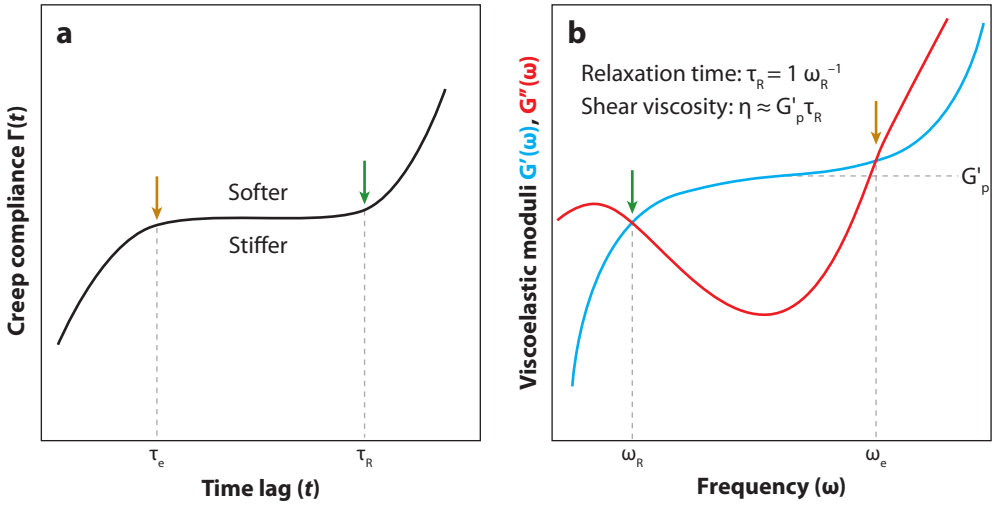

Figure 4

Creep compliance and viscoelastic moduli of the cytoplasm. (*a*) Typical creep compliance of the cytoplasm measured by the spontaneous displacements of beads embedded in the cytoplasm of a living cell (see also the inset in **Figure 2*c***). The creep compliance defines two characteristic timescales, τ_e and τ_R. (*b*) The frequency-dependent elastic (or storage) modulus, $G'(\omega)$, and viscous (or loss) modulus, $G''(\omega)$, of the cytoplasm can be approximately computed from the mean squared displacement of the beads or equivalently from the time-dependent creep compliance shown in panel *a*. In general, the cytoplasm behaves as a viscoelastic liquid at low frequencies (corresponding to long timescales, $t > \tau_R$): $G''(\omega) > G'(\omega)$ for $\omega < \omega_R$. The cytoplasm behaves as a viscoelastic solid at intermediate frequencies: $G'(\omega) > G''(\omega)$ for $\omega_e > \omega > \omega_R$. Finally, the cytoplasm behaves again as a viscous liquid at high frequencies: $\omega > \omega_e$, for which $G'(\omega) \sim G''(\omega) \sim \omega^{3/4}$.

Annu. Rev. Biophys. 2009.38:301-326. Downloaded from arjournals.annualreviews.org
by University of California - Berkeley on 04/07/10. For personal use only.

Annu. Rev. Biophys. 2009.38:301-326. Downloaded from arjournals.annualreviews.org
by University of California - Berkeley on 04/07/10. For personal use only.

inverse of the time required for lateral fluctuations to begin to touch the walls of the confining tube-like region (**Figure 4**).

In particle-tracking microrheology of living cells, the size of the probing beads is larger than the average mesh size of the cytoskeleton, typically 50 nm for fibroblasts (62, 63). Here again, without applying oscillatory deformations or mechanical stresses to the cytoplasm of the cells, the frequency-dependent elastic modulus and viscous modulus can be computed from the MSDs of embedded beads. In this case, the viscoelastic moduli can be obtained from the so-called complex modulus, $G^*(\omega)$, as (66)

$$G^*(\omega) = \frac{2k_B T}{3\pi a i \omega F_u[\Delta r^2(t)]}, \qquad 2.$$

where $F_u[\langle \Delta r^2(t)\rangle]$ is the unilateral Fourier transform of $\langle \Delta r^2(t)\rangle$. The above equation can be solved analytically (65), if we allow the frequency-dependent elastic modulus to be calculated algebraically using the following relationship:

$$G'(\omega) = |G^*(\omega)| \cos\left[\frac{\pi\alpha(\omega)}{2}\right], \qquad 3.$$

and the amplitude can be approximated as

$$|G^*(\omega)| \approx \frac{2k_B T}{3\pi a \langle \Delta r^2(1/\omega)\rangle \Gamma[1+\alpha(\omega)]}. \qquad 4.$$

Here α is the local logarithmic slope of $\langle \Delta r^2(t)\rangle$ estimated at the frequency of interest and Γ is the gamma function.

Dynamic Viscosity Versus Shear Viscosity

The viscous modulus (also called the loss modulus), $G''(\omega)$, or alternatively the dynamic viscosity, $\eta''(\omega) = G''(\omega)/\omega$, and the shear viscosity, η, of a material ought not to be confused with each other. $G''(\omega)$ has units of pressure (Pa or dyne/cm^2) and represents the fraction of the energy induced by the imposed deformation, which is lost by viscous dissipation as opposed to stored elastically by the material. In a rheometer, it is computed by imposing an oscillatory deformation of controlled frequency and measuring the out-of-phase component of the frequency-dependent stress induced in the material. In contrast, the shear viscosity η has units of Pa.s and is measured by imposing a steady deformation of constant rate. It is the ratio of the stress induced in the material to the rate of deformation.

Here again without applying any external forces to the cytoplasm, one can compute an approximate value of its shear viscosity η from the frequency-dependent viscoelastic moduli, $G'(\omega)$ and $G''(\omega)$:

$$\eta \approx G'_P \tau_R, \qquad 5.$$

where G'_P is the plateau value of the elastic modulus $G'(\omega)$ at intermediate frequencies (between ω_e and ω_R), and τ_R is the inverse of the frequency ω_R at which $G'(\omega)$ and $G''(\omega)$ are equal (see definitions in **Figure 4*a,b***). Typical values of shear viscosity of the cytoplasm are given in **Table 1**.

Particle-tracking microrheology not only shows that the rheology of the cytoplasm is timescale dependent, but also that the frequency-dependent viscoelastic moduli define a single crossover frequency, ω_R, at low frequencies (**Figure 4*b***). Below this frequency, the cytoplasm behaves essentially as a viscous liquid. Equivalently, in the time domain, if the cytoplasm were subjected to a step deformation, the time-dependent stress induced in the cytoplasm would adopt a plateau value at intermediate timescales, crossing over at a characteristic time τ_R $(= 1/\omega_R)$ to a terminal viscous relaxation at long timescales (15).

Creep Compliance from Particle-Tracking Measurements

From a rheological point of view, the cytoplasm is a viscoelastic material. As suggested above, the mathematical transformation of the measured time-dependent MSD into frequency-dependent elastic and viscous moduli, $G'(\omega)$ and $G''(\omega)$, is not trivial (65, 66) (see Equations 2–4). This transformation involves Fourier/Laplace integrals that presume the knowledge of the MSD over an infinite range of timescales. Therefore, large errors can

be introduced into the computation of $G'(\omega)$ and $G''(\omega)$ at low and high frequencies, corresponding to the maximum time of capture (at long timescales) and the rate of image capture of the camera for the MSD (at short timescales), respectively. However, the MSD of a bead is proportional to the creep compliance, $\Gamma(t)$, of the material in which the bead is embedded (114) (**Figures 2*c*** and **4*a***):

$$\Gamma(t) = \frac{3\pi a}{2k_B T}\langle \Delta r^2(t)\rangle. \qquad 6.$$

The creep compliance of a material is its deformability and, in classical rheological measurements, is obtained by imposing a steady mechanical stress of constant magnitude and measuring the resulting deformation of the material. Here we can compute the creep compliance from particle-tracking measurements without imposing any deformations.

If we return to the examples of viscous liquid and elastic solid described above, then simple substitution of the expressions of $\langle \Delta r^2\rangle$, $\langle \Delta r^2\rangle = (2k_B T/3\pi a\eta)t$ and $\langle \Delta r^2\rangle = K$ in Equation 6 indicates that the creep compliance of a viscous liquid is $\Gamma(t) = t/\eta$, while the creep compliance of a highly elastic solid (negligible viscosity) is $\Gamma(t) = (3\pi a K/2k_B T) =$ constant. Therefore, the creep compliance of a viscous liquid is inversely proportional to the shear viscosity, $\Gamma(t) \sim 1/\eta$, and the creep compliance of an elastic solid is the inverse of the material's elasticity, $\Gamma = 1/G'$, where G' is a constant.

All the rheological information about the cytoplasm or the material in which the probing beads are embedded is contained in both the time dependence of creep compliance and its magnitude (94) (**Figure 4*a***). To illustrate this, we return to the relatively simple example of a concentrated suspension of uncross-linked actin filaments, in which 100-nm-diameter beads have now been embedded. This bead is larger than the mesh size of the network. Hence the bead is in intimate physical contact with the filaments that, for a time, form a cage that confines the bead (**Figure 2*a***). At short timescales, the motion of the bead is dictated by the lateral fluctuations of the filaments in contact with the bead (**Figure 2*b***). Hence the MSD of the bead grows with time as $t^{3/4}$ (**Figure 2*c***). An ultrafast camera would show that the bead undergoes random, small-magnitude, rapid displacements created by the lateral fluctuations of the confining filaments. At intermediate timescales, the bead does not undergo net motion anymore. A camera capturing images at that rate would not capture any net motion of the bead because, at intermediate timescales, the filaments surrounding it cannot get out of their confining tube-like region. Finally, at long timescales, the filaments surrounding the bead can escape their tube-like regions through large-magnitude longitudinal motion (**Figure 2*b***). Accordingly, the filamentous cage that was confining the bead disappears because its constitutive filaments have moved out of the way. A slow camera would capture the bead going from cage to cage, undergoing a random walk—albeit at a slow pace set by the high viscosity of the actin filament solution. The MSD of the bead grows proportionally with time, a signature of viscous diffusion.

PARTICLE-TRACKING MICRORHEOLOGY OF CELLS

Interstitial Viscosity Versus Mesoscale Viscoelasticity of the Cytoplasm

The viscosity of the intracellular space depends critically on the length scale being probed. At small length scales, the viscosity of the cytoplasm is essentially that of water [more precisely, 1.2–1.4 times the viscosity of water (27)] or approximately 0.01 P (64, 91). It can be measured by monitoring the diffusion of GFP or small fluorescently labeled DNA fragments in the cell. This interstitial viscosity is a key parameter that controls the transport of small globular proteins and it varies slightly for various cell conditions.

At length scales larger than the effective mesh size of the cytoskeleton meshwork, the apparent viscosity is much higher, typically

Annu. Rev. Biophys. 2009.38:301-326. Downloaded from arjournals.annualreviews.org
by University of California - Berkeley on 04/07/10. For personal use only.

>10 P, or 1000 times the viscosity of water. This effective mesh size can be measured by probing the diffusion of fluorescently labeled dextran or DNA inside the cell. The diffusion of dextran polymers with a gyration radius of <50 nm within the cytoplasm (of fibroblasts) is largely unhindered, whereas polymers with a gyration radius of >50 nm become immobilized (63, 64, 91). At length scales larger than the effective mesh size of the cytoplasm, the viscoelastic moduli and creep compliance computed from particle-tracking measurements should be independent of the size of the probe beads used in the experiments. This is readily seen from the expression in Equation 1 in the limit case of a viscous liquid: The creep compliance depends linearly on both bead size and MSD, which itself depends inversely on bead size.

The above discussion about how viscoelastic parameters of the cytoplasm can be obtained from particle-tracking measurements assumes that the probing beads are larger than the effective mesh size of the cytoplasm or the network being probed (**Figure 4*a***). We call this viscosity mesoscale viscosity, as it describes the rheological properties at length scales intermediate between small globular proteins in the interstitial space and the whole cell. The mesoscale viscosity controls the rate of movements of mitochondria (53), nuclei (59), and phagosomes (96), as well as viruses, bacteria, and engineered drug delivery microcarriers (96), because these entities are larger than the effective mesh size of the cytoskeleton. The mesoscale viscosity of the cytoplasm also controls the rates of cell spreading and migration (35).

Active Versus Passive Microrheology

Direct injection of the beads into the cytoplasm (102), as opposed to passive engulfment of the beads inside the cytoplasm, circumvents the endocytic pathway and therefore the engulfment of the beads in vesicles tethered to cytoskeleton filaments by motor proteins (96). These vesicles move toward the nucleus; therefore, the probe beads undergo directed motion. Although interesting in their own right, such directed displacements prevent the computation of the viscoelastic parameters of the cytoplasm from MSDs.

Nevertheless, even in the absence of directed motion, actomyosin contractility could affect the movements of beads. Recent work with reconstituted actin filament networks containing myosin II has shown that in this in vitro system the movements of beads can be affected 10-fold, and even more at long timescales by the activity of motor proteins (69). Even without producing a net movement of the filaments, motor proteins enhance the random movements of the beads, akin to an effective >10-fold increase in the temperature of the system (69). These enhanced movements allow for faster relaxation of mechanical stresses. This result obtained with purified proteins suggests that particle-tracking measurements of the mechanical properties of the cytoplasm significantly underestimate the values of the viscoelastic properties of the cytoplasm in live cells.

However, our unpublished results suggest that reducing or eliminating actomyosin contractility in a live cell using either blebbistatin, which blocks the myosin heads in a complex with low actin affinity (52), or ML-7, which specifically inhibits MLCK (myosin light chain kinase), which normally phosphorylates myosin II, has no significant effect on the magnitude of the displacements of the beads compared with control cells. This absence of effect may result because myosin II molecules are mostly localized to the contractile actin stress fibers localized to the ventral side of the cell and the leading edge and are not present in large quantities in the body of the cell (108), where beads used for particle-tracking microrheology are lodged. Therefore, a direct extrapolation of results obtained in vitro with purified proteins, although often instructive of the more complex behavior of cytoskeleton in cells (79), can be misleading.

The movements of the cell itself can add an additional contribution to the overall movements of the probing beads. The speed of

Annu. Rev. Biophys. 2009.38:301-326. Downloaded from arjournals.annualreviews.org
by University of California - Berkeley on 04/07/10. For personal use only.

adherent cells (7) is typically much lower than the speed of the probing beads embedded in the cytoplasm. Therefore, the movements of the cell will be felt by the beads embedded in the cytoplasm only when they are monitored for a long time. The contribution of cell movements to the overall movements of the beads can readily be detected by the curvature of the MSDs of the embedded beads. To illustrate this effect, we consider the simple case of a viscous liquid. If an overall movement is added to the thermally driven random motion of the bead, then the MSD can be rewritten as (81)

$$\langle \Delta r^2 \rangle = 4Dt + \mathrm{v}^2 t^2, \qquad 7.$$

where v is the overall speed of the suspending liquid. The first term in this expression corresponds to the random thermally driven motion of the bead, and the second term corresponds to the motion of the bead imposed by the overall movement of the liquid. At short timescales, the second term is negligible and we recover $\langle \Delta r^2 \rangle \approx 4Dt$, i.e., bead movements are dominated by viscous diffusion. At long timescales, the second term dominates, $\langle \Delta r^2 \rangle \approx \mathrm{v}^2 t^2$, corresponding to a quadratic dependence on time, which is readily observed at long timescales in the MSD profile. The timescale at which the crossover between these two regimes occurs (when $4Dt = \mathrm{v}^2 t^2$) is $t = 4D/\mathrm{v}^2$. For instance, for a 100-nm-diameter bead in a 20 P viscous liquid, $D \approx 0.0022\ \mu\mathrm{m}^2/\mathrm{s}$, moving at a constant speed of 5 μm/h (a typical speed for a cultured adherent cell), the crossover time is equal to $t = 4D/\mathrm{v}^2 = 1.3$ s, which is readily detected when tracking a bead for 10 s.

Advantages of Particle-Tracking Microrheology Over Current Methods

Particle-tracking microrheology can measure directly the mechanical properties of the cytoplasm because of the intimate contact between the probing beads and subcellular structures (103). In contrast, most current single-cell mechanics methods rely on a direct contact between the cell surface and a physical probe. For example, AFM probes the mechanical properties of cells using soft cantilevers (41); magnetocytometry (106, 111) measures cell mechanics by subjecting large beads coated with extracellular matrix molecules bound to cell receptors to rotational movements. These methods cannot distinguish the contribution of the plasma membrane from the combined response of the nucleus and the cytoplasm without making drastic assumptions. If two elastic elements of different stiffness are connected to one another (here the nucleus and the cytoskeleton), their total response is dominated by the stiffer element. Therefore, methods such as AFM, magnetocytometry, or micropipette suction probe the combined response of the nucleus and cytoplasm, even when the probe is positioned far away from the nucleus. In contrast, particle-tracking microrheology, which relies on the smallest energy possible—thermal energy—is a highly localized measurement inside the cytoplasm.

Unlike most other approaches to cell mechanics, particle-tracking microrheology measures frequency-rate-dependent viscoelastic moduli, $G'(\omega)$ and $G''(\omega)$. This is particularly crucial for the cytoskeleton, which behaves like a liquid at long timescales (or low rates of shear) and like an elastic solid at short timescales (or high rates of shear). The frequency-dependent mechanical response of the cytoplasm of a live cell can be measured in about 10 s by particle-tracking microrheology, at least for timescales relevant to cell motility. In contrast, AFM measurements may take up to 1 h for high-resolution mechanical measurements (82). Such time-consuming measurements cannot capture fast subcellular dynamics and are unsuitable for motile cells.

Particle-tracking microrheology requires short times of data collection, typically 10–20 s, to measure frequency-dependent viscoelastic moduli over two decades in frequency (or timescales). This is not the case for other particle-tracking methods for which the correlated motion between two particles is used instead of the motion of individual particles as a probe of local cytoplasmic rheology (13). These methods are inappropriate for the

Annu. Rev. Biophys. 2009.38:301-326. Downloaded from arjournals.annualreviews.org
by University of California - Berkeley on 04/07/10. For personal use only.

Annu. Rev. Biophys. 2009.38:301-326. Downloaded from arjournals.annualreviews.org
by University of California - Berkeley on 04/07/10. For personal use only.

measurement of the mechanical properties of live cells because they incorrectly assume that the intracellular milieu is homogeneous and static. Furthermore, to obtain statistically significant data, measurement times are on the order of 30–60 min, timescales for which migrating cells cannot be assumed to be stationary.

By tracking multiple beads simultaneously, microrheology can measure simultaneously the micromechanical responses to stimuli in various parts of the cell. This is particularly important because the viscoelastic properties can vary by more than 2 orders of magnitude within the same cell (51, 102, 103). By using video-based, multiple-particle tracking instead of laser-deflection particle tracking (65, 116), hundreds of beads embedded in the cytoplasm can be tracked at the same time.

Particle-tracking microrheology measurements of the cytoplasm of live cells are typically conducted using carboxylated polystyrene beads or polyethylene glycol (PEG)-coated beads. The rheology of reconstituted actin filament networks or DNA solutions measured by particle-tracking microrheology and using these beads is quantitatively similar to that measured by rheometry (75, 114). This indicates that the presence of the beads in polymer networks does not affect the global mechanical properties of the networks. Moreover, our unpublished results show that carboxylated polystyrene beads or PEG-coated beads yield the same frequency-dependent viscoelastic moduli for the cytoplasm of fibroblasts, but not for amino-modified beads (102). Finally, the proximity of some of the beads to the plasma membrane will not significantly affect the movements of the beads because hydrodynamic interactions caused by the movements of the beads and reflecting off the membrane are effectively screened by the cytoskeleton mesh (21, 116). Subcellular organelles can also be used as probing particles (40, 86, 116). However, because their interactions with subcellular structures are ill-defined, only the frequency dependence of the viscoelastic moduli is meaningful, at least at high frequency, not the absolute value of moduli.

Microrheological measurements are absolute and compare favorably with traditional rheometric measurements of standard fluids of known viscosity and elasticity (2, 65, 112, 114). This is not the case of some single-cell approaches that rely on a direct physical contact between the cell surface and the probe (such as a cantilever or a macroscopic bead). For instance, the apparent viscoelastic moduli measured by magnetocytometry and AFM depend greatly on the type of ligands coated on the magnetic beads or the AFM cantilever. Extracellular matrix ligands—including fibronectin or RGD peptide—coated onto magnetic beads and AFM cantilevers lead to vastly different values of (apparent) cell stiffness. Therefore, the measurements of viscoelastic properties of standard materials using these methods cannot be readily compared with those obtained using a rheometer. Furthermore, particle-tracking microrheology measures both elasticity and viscosity, whereas many other approaches cannot directly distinguish the elastic response from the viscous response of the cell.

Importantly, values of shear viscosity and elastic moduli of the cytoplasm in live cells measured by particle-tracking microrheology (**Table 1**) are similar to those measured in reconstituted actin filament networks in the presence of cross-linking/bundling proteins (**Table 2**). The elasticity of live cells, such as mouse embryonic fibroblasts or human umbilical vein endothelial cells (HUVECs), which are commonly used as models of cell biology, and of reconstituted actin filament networks are on the order of tens of Pascal (hundreds of dyne per cm^2). This is in striking contrast to values of cell elasticity obtained using AFM, which is of the order of hundreds and even thousands of Pascal (82). To our knowledge, no actin filament network reconstituted in vitro that contains a physiological concentration of actin polymerized in the presence of cross-linking and bundling proteins and under mechanical tension (which can further increase the network elasticity) reaches these high levels of elasticity (99). The discrepancy between values of cell elasticity measured by AFM and those obtained

Table 2 Viscosity and elasticity of common liquids and cytoskeletal filament networks measured by a cone-and-plate rheometer

Type of material; values of viscoelastic parameters	Average viscosity (poise)	Average elasticity at 1 rad/s (dyne/cm^2)	Reference
Water	0.01	0	–
Blood	0.1	Negligible	–
Glycerol	~1	Negligible	–
Corn syrup	~20	Negligible	–
Ketchup	~500	Negligible	–
Jell-O	Negligible	1,000	–
Polyacrylamide gel	–	500	(26)
F-actin network	–	8 ± 3	(113)
F-actin + filamin	–	450 ± 60	(99)
F-actin + α-actinin	–	120 ± 20	(113)
F-actin + Arp2/3 complex/WASp	–	60 ± 15	(105)
F-actin + fascin	–	80 ± 10	(101)
F-actin + fimbrin	–	300 ± 30	(48)
Vimentin network	–	14 ± 2	(23)

[a]Measurements are mean ± sem. The elasticity was measured at a shear amplitude of 1% and a shear frequency of 1 rad/s. Shear viscosity of the F-actin and vimentin networks was not measured because these filaments break under continuous shear.

[b]The concentrations of actin and vimentin solutions are 24 μM. The concentrations of α-actinin, fascin, fimbrin, and filamin in solutions are 0.24 μM. The concentration of the Arp2/3 complex is 0.12 μM and that of its activator WASp is 0.06 μM. The concentration of acrylamide and bis-acrylamide in the polyacrylamide gel is 0.04% and 0.05%, respectively. Unit conversions are 1 P = 0.1 Pa.s; 1 dyne/cm^2 = 0.1 Pa.

Annu. Rev. Biophys. 2009.38:301-326. Downloaded from arjournals.annualreviews.org
by University of California - Berkeley on 04/07/10. For personal use only.

with actin filament networks by conventional rheometry or particle-tracking microrheology remains unexplained.

Applications of particle-tracking microrheology discussed in the Introduction were rendered possible thanks to the replacement of manual microinjection of beads into cells with ballistic injection (61, 76, 77). In a single ballistic injection, the number of injected cells amenable to measurements increases 1000-fold compared with conventional microinjection (61, 77). With a large sample size per condition (typical number of probed cells is ~30), particle-tracking microrheology results become more precise and significant. Ballistic transfer of beads to the cytoplasm coupled with particle tracking (named ballistic injection nanorheology, or BIN) provides a more precise and consistent value for global and local viscoelastic properties.

Illustrative Example of Particle-Tracking Microrheology of Living Cells

In typical measurements of cell mechanics (e.g., AFM) (82–84), it is assumed that the nucleus and the cytoplasm contribute independently to global cell stiffness. This assumption is an oversimplification that overlooks the existence of critical functional links between the nucleus and the cytoskeleton. These connections are established by specific linker proteins located at the nuclear envelope, including the LINC complex (10), and they physically connect the filamentous nuclear lamina underneath the nuclear envelope to the actin/microtubule/intermediate filament cytoskeleton in the cytoplasm. These physical connections between nucleus and cytoskeleton are as important to cell mechanics as the intrinsic mechanical properties of the nucleus and the cytoskeleton themselves. Indeed,

when these functional links are disrupted, the elasticity of the cytoplasm is drastically reduced; the magnitude of this reduction is as important as when the actin cytoskeleton is completely disassembled with drugs (60).

Particle-tracking microrheology shows that the loss of the LINC complex dramatically affects the ability of cells to resist mechanical shear forces (95). Mutations scattered along *Lmna*, which encodes A-type lamins, have been associated with a broad range of human diseases collectively called laminopathies (4, 8, 9, 33, 42, 71). These diseases involve either specific or combined pathologies of neurons, muscle, and bone tissue (4, 42). Cytoplasmic fragility as measured by particle-tracking microrheology correlates with the loss of the LINC complex from the nuclear envelope in cells derived from mouse models of laminopathy (37, 60, 95) (**Figure 5**).

Annu. Rev. Biophys. 2009.38:301-326. Downloaded from arjournals.annualreviews.org
by University of California - Berkeley on 04/07/10. For personal use only.

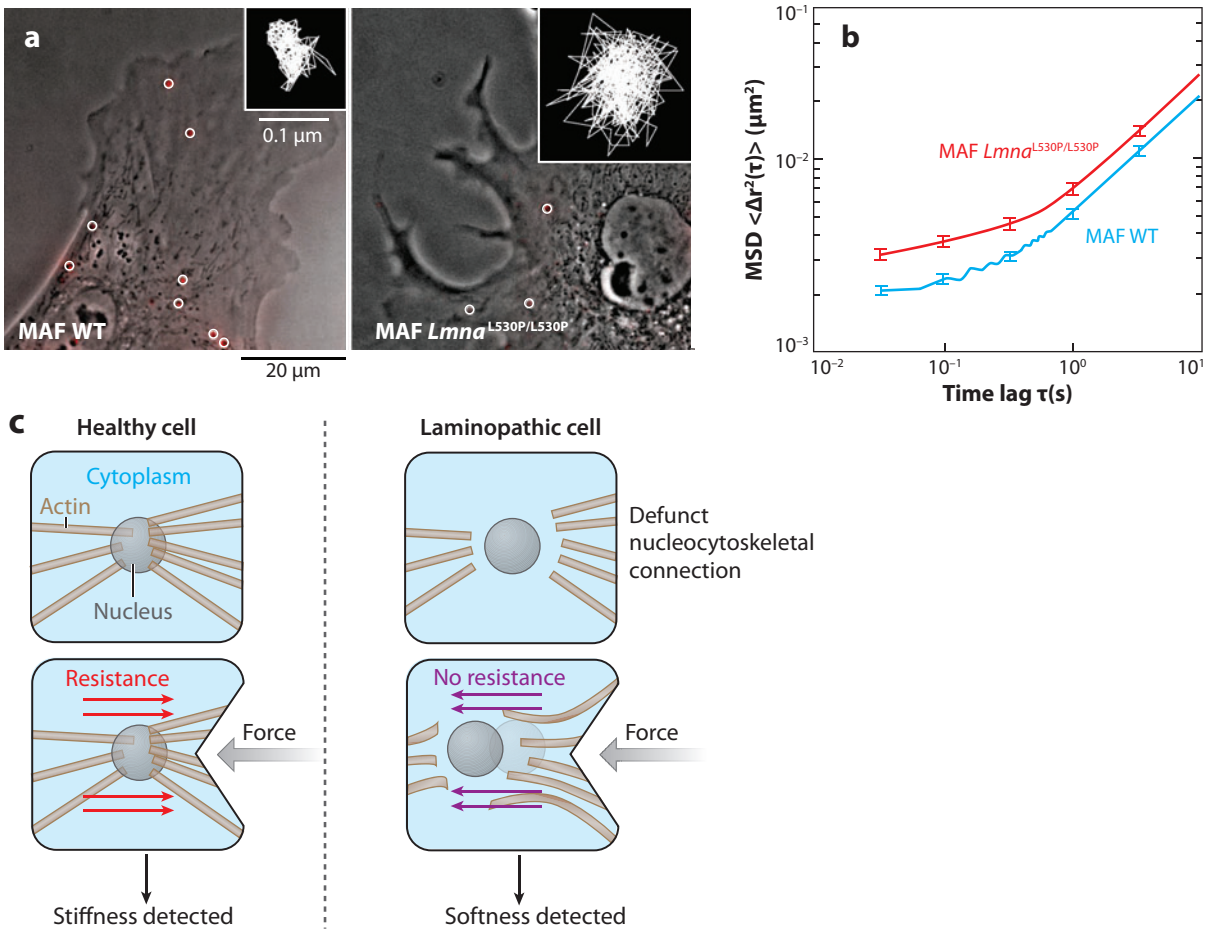

Figure 5

Intracellular microrheology of laminopathic fibroblasts. (*a*) Fluorescent 100-nm-diameter polystyrene beads are ballistically injected into wild-type (WT) (*left panel*) and *Lmna*$^{L530P/L530P}$ (*right panel*) mouse adult fibroblasts (MAFs), derived from a mouse model of progeria. Fluorescent micrographs of beads (*outlined in white circles*) are superimposed onto phase-contrast micrographs of cells. Representative trajectories of nanoparticles are shown at the top right of each micrograph (*inset*). (*b*) Ensemble-averaged mean squared displacements (MSDs) of the beads embedded in the cytoplasm of WT (*blue curve*) and *Lmna*$^{L530P/L530P}$ (*red curve*) MAFs are shown. (*c*) Model for the intracellular mechanics of healthy and laminopathic cells. Healthy cells in which the nucleocytoskeletal connections are intact can resist forces of large magnitude, whereas laminopathic cells cannot resist such forces because of defunct nucleocytoskeletal connections. Modified with permission from Reference 37.

Annu. Rev. Biophys. 2009.38:301-326. Downloaded from arjournals.annualreviews.org
by University of California - Berkeley on 04/07/10. For personal use only.

SUMMARY POINTS

1. The viscoelastic properties of the cytoplasm and nucleoplasm control key cell functions, including cell motility, cell adhesion, and the regulated movements of organelles.
2. Particle-tracking microrheology can measure the viscoelastic properties of living cells without subjecting them to applied forces. In this approach, fluorescent submicron beads are injected directly into the cytoplasm of live cells. These beads rapidly disperse throughout the cytoplasm and are subsequently tracked by fluorescence microscopy. Analysis of the recorded movements of the beads transforms the MSDs of the beads in terms of either viscosity and elasticity or the compliance of the cytoplasm.
3. Particle-tracking microrheology can reveal the micromechanical properties of cells in more physiological environments, such as a 3D extracellular matrix or inside an embryo, better than traditional approaches to cell mechanics.
4. Particle-tracking microrheology measurements, which are fast, acknowledge that the mechanical properties of the cytoplasm are spatially variable and depend on timescale.
5. Particle-tracking microrheology reveals the reduced ability of cells from mouse models of laminopathies to resist mechanical shear forces.

FUTURE ISSUES

1. The levels of viscosity, elasticity, and compliance of the cytoplasm, as measured by particle-tracking microrheology, should be tested to determine whether they can serve as reliable diagnostic markers of disease, in particular cancer and laminopathies.
2. To circumvent the need of beads to probe cytoplasmic microrheology, exogenous beads should be rationally replaced with endogenous subcellular markers.
3. Researchers should assess quantitatively the role of motor proteins (e.g., myosins) on the movements of beads lodged in the cytoskeleton of living cells and therefore the computation of viscoelastic parameters.
4. Can the wide range of phenotypes associated with human laminopathy be explained by the differential mechanical response at the cellular level?
5. A high-throughput device based on particle-tracking microrheology would allow the method to become a diagnostic tool for human disease.
6. Particle-tracking microrheology should be extended to in vivo measurements.

DISCLOSURE STATEMENT

The author is not aware of any biases that might be perceived as affecting the objectivity of this review.

ACKNOWLEDGMENTS

The author thanks Yiider Tseng, Thomas P. Kole, Jerry S.H. Lee, Porntula Panorchan, Brian R. Daniels, and Melissa S. Thompson for key contributions to the development of particle-tracking

microrheology and its applications in cell biology, as well as Didier Hodzic, Christopher M. Hale, Shyam B. Khatau, Philip Stewart-Hutchinson, and Colin L. Stewart, who contributed to the work on nucleocytoskeleton protein linkers. The author also thanks members of the Wirtz group for reading and editing the manuscript. Work in the author's laboratory is supported by the National Institutes of Health (NIGMS, NIBIB, and NCI), the Howard Hughes Medical Institute, and the American Heart Association.

LITERATURE CITED

1. Alberts B, Bray D, Lewis J, Raff M, Roberts K, Watson JD. 1994. *Molecular Biology of the Cell*. New York: Garland. 1408 pp.
2. Apgar J, Tseng Y, Federov E, Herwig MB, Almo SC, Wirtz D. 2000. Multiple-particle tracking measurements of heterogeneities in solutions of actin filaments and actin bundles. *Biophys. J.* 79:1095–106
3. Bausch AR, Kroy K. 2006. A bottom-up approach to cell mechanics. *Nat. Phys.* 2:231–38
4. Ben Yaou R, Muchir A, Arimura T, Massart C, Demay L, et al. 2005. Genetics of laminopathies. *Novartis Found. Symp.* 264:81–90
5. Berg HC. 1993. *Random Walks in Biology*. Princeton, NJ: Princeton Univ. Press. 152 pp.
6. Bloom RJ, George JP, Celedon A, Sun SX, Wirtz D. 2008. Mapping local matrix remodeling induced by a migrating tumor cell using three-dimensional multiple-particle tracking. *Biophys. J.* 95:4077–88
7. Bray D. 2001. *Cell Movements: From Molecules to Motility*. New York: Garland. 371 pp.
8. Broers JL, Hutchison CJ, Ramaekers FC. 2004. Laminopathies. *J. Pathol.* 204:478–88
9. Capell BC, Collins FS. 2006. Human laminopathies: Nuclei gone genetically awry. *Nat. Rev. Genet.* 7:940–52
10. Crisp M, Liu Q, Roux K, Rattner JB, Shanahan C, et al. 2006. Coupling of the nucleus and cytoplasm: role of the LINC complex. *J. Cell Biol.* 172:41–53
11. Crocker JC, Grier DG. 1996. Methods of digital video microscopy for colloidal studies. *J. Colloid Interface Sci.* 179:298–310
12. Crocker JC, Hoffman BD. 2007. Multiple-particle tracking and two-point microrheology in cells. *Methods Cell Biol.* 83:141–78
13. Crocker JC, Valentine MT, Weeks ER, Gisler T, Kaplan PD, et al. 2000. Two-point microrheology of inhomogeneous soft materials. *Phys. Rev. Lett.* 85:888–91
14. Cross SE, Jin YS, Rao J, Gimzewski JK. 2007. Nanomechanical analysis of cells from cancer patients. *Nat. Nanotechnol.* 2:780–83
15. Dahl KN, Engler AJ, Pajerowski JD, Discher DE. 2005. Power-law rheology of isolated nuclei with deformation mapping of nuclear substructures. *Biophys. J.* 89:2855–64
16. Daniels BR, Masi BC, Wirtz D. 2006. Probing single-cell micromechanics in vivo: the microrheology of *C. elegans* developing embryos. *Biophys. J.* 90:4712–19
17. de Gennes P-G. 1991. *Scaling Concepts in Polymer Physics*. Ithaca, NY: Cornell Univ. Press
18. de Gennes P-G, Leger L. 1982. Dynamics of entangled polymer chains. *Annu. Rev. Phys. Chem.* 33:49–61
19. Desai KV, Bishop TG, Vicci L, O'Brien ET Sr, Taylor RM 2nd, Superfine R. 2008. Agnostic particle tracking for three-dimensional motion of cellular granules and membrane-tethered bead dynamics. *Biophys. J.* 94:2374–84
20. Discher DE, Janmey P, Wang YL. 2005. Tissue cells feel and respond to the stiffness of their substrate. *Science* 310:1139–43
21. Doi M, Edwards SF. 1989. *The Theory of Polymer Dynamics*. Oxford: Clarendon. 391 pp.
22. Engler AJ, Sen A, Sweeney HL, Discher DE. 2006. Matrix elasticity directs stem cell lineage specification. *Cell* 126:677–89
23. Esue O, Carson AA, Tseng Y, Wirtz D. 2006. A direct interaction between actin and vimentin filaments mediated by the tail domain of vimentin. *J. Biol. Chem.* 281:30393–99
24. Ferry JD. 1980. *Viscoelastic Properties of Polymers*. New York: Wiley. 672 pp.
25. Flanagan LA, Chou J, Falet H, Neujahr R, Hartwig JH, Stossel TP. 2001. Filamin A, Arp2/3 complex, and the morphology and function of cortical actin filaments in human melanoma cells. *J. Cell Biol.* 155:511–18

Annu. Rev. Biophys. 2009.38:301-326. Downloaded from arjournals.annualreviews.org
by University of California - Berkeley on 04/07/10. For personal use only.

26. Flanagan LA, Ju YE, Marg B, Osterfield M, Janmey PA. 2002. Neurite branching on deformable substrates. *NeuroReport* 13:2411–17
27. Fushimi K, Verkman AS. 1991. Low viscosity in the aqueous domain of cell cytoplasm measured by picosecond polarization microfluorimetry. *J. Cell Biol.* 112:719–25
28. Girard KD, Chaney C, Delannoy M, Kuo SC, Robinson DN. 2004. Dynacortin contributes to cortical viscoelasticity and helps define the shape changes of cytokinesis. *EMBO J.* 23:1536–46
29. Girard KD, Kuo SC, Robinson DN. 2006. *Dictyostelium* myosin II mechanochemistry promotes active behavior of the cortex on long time scales. *Proc. Natl. Acad. Sci. USA* 103:2103–8
30. Gittes F, Mickey B, Nettleton J, Howard J. 1993. Flexural rigidity of microtubules and actin filaments measured from thermal fluctuations in shape. *J. Cell Biol.* 120:923–34
31. Gomes ER, Jani S, Gundersen GG. 2005. Nuclear movement regulated by Cdc42, MRCK, myosin, and actin flow establishes MTOC polarization in migrating cells. *Cell* 121:451–63
32. Gorisch SM, Wachsmuth M, Ittrich C, Bacher CP, Rippe K, Lichter P. 2004. Nuclear body movement is determined by chromatin accessibility and dynamics. *Proc. Natl. Acad. Sci. USA* 101:13221–26
33. Gruenbaum Y, Margalit A, Goldman RD, Shumaker DK, Wilson KL. 2005. The nuclear lamina comes of age. *Nat. Rev. Mol. Cell. Biol.* 6:21–31
34. Guck J, Schinkinger S, Lincoln B, Wottawah F, Ebert S, et al. 2005. Optical deformability as an inherent cell marker for testing malignant transformation and metastatic competence. *Biophys. J.* 88:3689–98
35. Gupton SL, Anderson KL, Kole TP, Fischer RS, Ponti A, et al. 2005. Cell migration without a lamellipodium: translation of actin dynamics into cell movement mediated by tropomyosin. *J. Cell Biol.* 168:619–31
36. Haber C, Ruiz SA, Wirtz D. 2000. Shape anisotropy of a single random-walk polymer. *Proc. Natl. Acad. Sci. USA* 97:10792–95
37. Hale CM, Shrestha AL, Khatau SB, Stewart-Hutchinson PJ, Hernandez L, et al. 2008. Dysfunctional connections between the nucleus and the actin and microtubule networks in laminopathic models. *Biophys. J.* 95:5462–75
38. Hasnain IA, Donald AM. 2006. Microrheological characterization of anisotropic materials. *Phys. Rev. E* 73:031901
39. Hinner B, Tempel M, Sackmann E, Kroy K, Frey E. 1998. Entanglement, elasticity, and viscous relaxation of actin solutions. *Phys. Rev. Lett.* 81:2614–17
40. Hoffman BD, Massiera G, Van Citters KM, Crocker JC. 2006. The consensus mechanics of cultured mammalian cells. *Proc. Natl. Acad. Sci. USA* 103:10259–64
41. Hoh JH, Schoenenberger CA. 1994. Surface morphology and mechanical properties of MDCK monolayers by atomic force microscopy. *J. Cell Sci.* 107(Pt. 5):1105–14
42. Jacob KN, Garg A. 2006. Laminopathies: multisystem dystrophy syndromes. *Mol. Genet. Metab.* 87:289–302
43. Janmey PA. 1991. Mechanical properties of cytoskeletal polymers. *Curr. Opin. Cell Biol.* 2:4–11
44. Janmey PA, Hvidt S, Lamb J, Stossel TP. 1990. Resemblance of actin-binding protein/actin gels to covalently crosslinked networks. *Nature* 345:89–92
45. Jonas M, Huang H, Kamm RD, So PT. 2008. Fast fluorescence laser tracking microrheometry. II. Quantitative studies of cytoskeletal mechanotransduction. *Biophys. J.* 95:895–909
46. Kas J, Strey H, Sackmann E. 1994. Direct imaging of reptation for semiflexible actin filaments. *Nature* 368:226–29
47. Kas J, Strey H, Tang JX, Fanger D, Sackmann E, Janmey P. 1996. F-actin, a model polymer for semiflexible chains in dilute, semidilute, and liquid crystalline solutions. *Biophys. J.* 70:609–25
48. Klein MG, Shi W, Ramagopal U, Tseng Y, Wirtz D, et al. 2004. Structure of the actin crosslinking core of fimbrin. *Structure* 12:999–1013
49. Kole TP, Tseng Y, Huang L, Katz JL, Wirtz D. 2004. Rho kinase regulates the intracellular micromechanical response of adherent cells to rho activation. *Mol. Biol. Cell* 15:3475–84
50. Kole TP, Tseng Y, Jiang I, Katz JL, Wirtz D. 2005. Intracellular mechanics of migrating fibroblasts. *Mol. Biol. Cell* 16:328–38
51. Kole TP, Tseng Y, Wirtz D. 2004. Intracellular microrheology as a tool for the measurement of the local mechanical properties of live cells. *Methods Cell Biol.* 78:45–64

Annu. Rev. Biophys. 2009.38:301-326. Downloaded from arjournals.annualreviews.org
by University of California - Berkeley on 04/07/10. For personal use only.

52. Kovacs M, Toth J, Hetenyi C, Malnasi-Csizmadia A, Sellers JR. 2004. Mechanism of blebbistatin inhibition of myosin II. *J. Biol. Chem.* 279:35557–63
53. Lacayo CI, Theriot JA. 2004. *Listeria* monocytogenes actin-based motility varies depending on subcellular location: a kinematic probe for cytoarchitecture. *Mol. Biol. Cell* 15:2164–75
54. Lammerding J, Lee RT. 2005. The nuclear membrane and mechanotransduction: impaired nuclear mechanics and mechanotransduction in lamin A/C deficient cells. *Novartis Found. Symp.* 264:264–73
55. Lammerding J, Schulze PC, Takahashi T, Kozlov S, Sullivan T, et al. 2004. Lamin A/C deficiency causes defective nuclear mechanics and mechanotransduction. *J. Clin. Invest.* 113:370–78
56. Lammermann T, Bader BL, Monkley SJ, Worbs T, Wedlich-Soldner R, et al. 2008. Rapid leukocyte migration by integrin-independent flowing and squeezing. *Nature* 453:51–55
57. Lau AW, Hoffman BD, Davies A, Crocker JC, Lubensky TC. 2003. Microrheology, stress fluctuations, and active behavior of living cells. *Phys. Rev. Lett.* 91:198101
58. Lee GY, Lim CT. 2007. Biomechanics approaches to studying human diseases. *Trends Biotechnol.* 25:111–18
59. Lee JS, Chang MI, Tseng Y, Wirtz D. 2005. Cdc42 mediates nucleus movement and MTOC polarization in Swiss 3T3 fibroblasts under mechanical shear stress. *Mol. Biol. Cell* 16:871–80
60. Lee JS, Hale CM, Panorchan P, Khatau SB, George JP, et al. 2007. Nuclear lamin A/C deficiency induces defects in cell mechanics, polarization, and migration. *Biophys. J.* 93:2542–52
61. Lee JS, Panorchan P, Hale CM, Khatau SB, Kole TP, et al. 2006. Ballistic intracellular nanorheology reveals ROCK-hard cytoplasmic stiffening response to fluid flow. *J. Cell Sci.* 119:1760–68
62. Luby-Phelps K, Castle PE, Taylor DL, Lanni F. 1987. Hindered diffusion of inert tracer particles in the cytoplasm of mouse 3T3 cells. *Proc. Natl. Acad. Sci. USA* 84:4910–13
63. Luby-Phelps K, Taylor DL, Lanni F. 1986. Probing the structure of cytoplasm. *J. Cell Biol.* 102:2015–22
64. Lukacs GL, Haggie P, Seksek O, Lechardeur D, Freedman N, Verkman AS. 2000. Size-dependent DNA mobility in cytoplasm and nucleus. *J. Biol. Chem.* 275:1625–29
65. Mason TG, Ganesan K, van Zanten JV, Wirtz D, Kuo SC. 1997. Particle-tracking microrheology of complex fluids. *Phys. Rev. Lett.* 79:3282–85
66. Mason TG, Weitz D. 1995. Optical measurements of frequency-dependent linear viscoelastic moduli of complex fluids. *Phys. Rev. Lett.* 74:1254–56
67. Massiera G, Van Citters KM, Biancaniello PL, Crocker JC. 2007. Mechanics of single cells: rheology, time dependence, and fluctuations. *Biophys. J.* 93:3703–13
68. Minin AA, Kulik AV, Gyoeva FK, Li Y, Goshima G, Gelfand VI. 2006. Regulation of mitochondria distribution by RhoA and formins. *J. Cell Sci.* 119:659–70
69. Mizuno D, Tardin C, Schmidt CF, Mackintosh FC. 2007. Nonequilibrium mechanics of active cytoskeletal networks. *Science* 315:370–73
70. Morse DC. 1998. Viscoelasticity of concentrated isotropic solutions of semiflexible polymers. 1. Model and stress tensor. *Macromolecules* 31:7030–43
71. Mounkes L, Kozlov S, Burke B, Stewart CL. 2003. The laminopathies: nuclear structure meets disease. *Curr. Opin. Genet. Dev.* 13:223–30
72. O'Toole M, Lamoureux P, Miller KE. 2008. A physical model of axonal elongation: force, viscosity, and adhesions govern the mode of outgrowth. *Biophys. J.* 94:2610–20
73. Pai A, Sundd P, Tees DF. 2008. In situ microrheological determination of neutrophil stiffening following adhesion in a model capillary. *Ann. Biomed. Eng.* 36:596–603
74. Palmer A, Xu J, Kuo SC, Wirtz D. 1999. Diffusing wave spectroscopy microrheology of actin filament networks. *Biophys. J.* 76:1063–71
75. Palmer A, Xu J, Wirtz D. 1998. High-frequency rheology of crosslinked actin networks measured by diffusing wave spectroscopy. *Rheol. Acta* 37:97–108
76. Panorchan P, Lee JS, Daniels BR, Kole TP, Tseng Y, Wirtz D. 2007. Probing cellular mechanical responses to stimuli using ballistic intracellular nanorheology. *Methods Cell Biol.* 83:115–40
77. Panorchan P, Lee JS, Kole TP, Tseng Y, Wirtz D. 2006. Microrheology and ROCK signaling of human endothelial cells embedded in a 3D matrix. *Biophys. J.* 91:3499–507
78. Pelham RJ Jr, Wang Y. 1997. Cell locomotion and focal adhesions are regulated by substrate flexibility. *Proc. Natl. Acad. Sci. USA* 94:13661–65

Annu. Rev. Biophys. 2009.38:301-326. Downloaded from arjournals.annualreviews.org
by University of California - Berkeley on 04/07/10. For personal use only.

79. Pollard TD. 2003. The cytoskeleton, cellular motility and the reductionist agenda. *Nature* 422:741–45
80. Pollard TD, Borisy GG. 2003. Cellular motility driven by assembly and disassembly of actin filaments. *Cell* 112:453–65
81. Qian H, Sheetz MP, Elson EL. 1991. Single particle tracking. Analysis of diffusion and flow in two-dimensional systems. *Biophys. J.* 60:910–21
82. Radmacher M. 2007. Studying the mechanics of cellular processes by atomic force microscopy. *Methods Cell Biol.* 83:347–72
83. Radmacher M, Cleveland JP, Fritz M, Hansma HG, Hansma PK. 1994. Mapping interaction forces with the atomic force microscope. *Biophys. J.* 66:2159–65
84. Radmacher M, Fritz M, Kacher CM, Cleveland JP, Hansma PK. 1996. Measuring the viscoelastic properties of human platelets with the atomic force microscope. *Biophys. J.* 70:556–67
85. Rogers SS, Waigh TA, Lu JR. 2008. Intracellular microrheology of motile *Amoeba proteus*. *Biophys. J.* 94:3313–22
86. Rogers SS, Waigh TA, Zhao X, Lu JR. 2007. Precise particle tracking against a complicated background: polynomial fitting with Gaussian weight. *Phys. Biol.* 4:220–27
87. Rudnick J, Gaspari G. 1987. The shapes of random walks. *Science* 237:384–89
88. Savin T, Doyle PS. 2005. Role of a finite exposure time on measuring an elastic modulus using microrheology. *Phys. Rev. E* 71:041106
89. Savin T, Doyle PS. 2005. Static and dynamic errors in particle tracking microrheology. *Biophys. J.* 88:623–38
90. Schnurr B, Gittes F, MacKintosh FC, Schmidt CF. 1997. Determining microscopic viscoelasticity in flexible and semiflexible polymer networks from thermal fluctuations. *Macromolecules* 30:7781–92
91. Seksek O, Biwersi J, Verkman AS. 1997. Translational diffusion of macromolecule-sized solutes in cytoplasm and nucleus. *J. Cell Biol.* 138:131–42
92. Sivaramakrishnan S, DeGiulio JV, Lorand L, Goldman RD, Ridge KM. 2008. Micromechanical properties of keratin intermediate filament networks. *Proc. Natl. Acad. Sci. USA* 105:889–94
93. Smith SB, Finzi L, Bustamante C. 1992. Direct mechanical measurements of the elasticity of single DNA molecules by using magnetic beads. *Science* 258:1122–26
94. Stamenovic D, Rosenblatt N, Montoya-Zavala M, Matthews BD, Hu S, et al. 2007. Rheological behavior of living cells is timescale-dependent. *Biophys. J.* 93:L39–41
95. Stewart-Hutchinson PJ, Hale CM, Wirtz D, Hodzic D. 2008. Structural requirements for the assembly of LINC complexes and their function in cellular mechanical stiffness. *Exp. Cell Res.* 314:1892–905
96. Suh J, Wirtz D, Hanes J. 2003. Efficient active transport of gene nanocarriers to the cell nucleus. *Proc. Natl. Acad. Sci. USA* 100:3878–82
97. Svitkina TM, Verkhovsky AB, McQuade KM, Borisy GG. 1997. Analysis of the actin-myosin II system in fish epidermal keratocytes: mechanism of cell body translocation. *J. Cell Biol.* 139:397–414
98. Tapon N, Hall A. 1997. Rho, Rac and Cdc42 GTPases regulate the organization of the actin cytoskeleton. *Curr. Opin. Cell Biol.* 9:86–92
99. Tseng Y, An KM, Esue O, Wirtz D. 2004. The bimodal role of filamin in controlling the architecture and mechanics of F-actin networks. *J. Biol. Chem.* 279:1819–26
100. Tseng Y, An KM, Wirtz D. 2002. Microheterogeneity controls the rate of gelation of actin filament networks. *J. Biol. Chem.* 277:18143–50
101. Tseng Y, Fedorov E, McCaffery JM, Almo SC, Wirtz D. 2001. Micromechanics and microstructure of actin filament networks in the presence of the actin-bundling protein human fascin: a comparison with α-actinin. *J. Mol. Biol.* 310:351–66
102. Tseng Y, Kole TP, Wirtz D. 2002. Micromechanical mapping of live cells by multiple-particle-tracking microrheology. *Biophys. J.* 83:3162–76
103. Tseng Y, Lee JS, Kole TP, Jiang I, Wirtz D. 2004. Micro-organization and visco-elasticity of the interphase nucleus revealed by particle nanotracking. *J. Cell Sci.* 117:2159–67
104. Tseng Y, Wirtz D. 2001. Mechanics and multiple-particle tracking microheterogeneity of alpha-actinin-cross-linked actin filament networks. *Biophys. J.* 81:1643–56
105. Tseng Y, Wirtz D. 2004. Dendritic branching and homogenization of actin networks mediated by Arp2/3 complex. *Phys. Rev. Lett.* 93:258104

Annu. Rev. Biophys. 2009.38:301-326. Downloaded from arjournals.annualreviews.org
by University of California - Berkeley on 04/07/10. For personal use only.

106. Valberg PA, Albertini DF. 1985. Cytoplasmic motions, rheology, and structure probed by a novel magnetic particle method. *J. Cell Biol.* 101:130–40
107. Van Citters KM, Hoffman BD, Massiera G, Crocker JC. 2006. The role of F-actin and myosin in epithelial cell rheology. *Biophys. J.* 91:3946–56
108. Verkhovsky AB, Svitkina TM, Borisy GG. 1995. Myosin II filament assemblies in the active lamella of fibroblasts: their morphogenesis and role in the formation of actin filament bundles. *J. Cell Biol.* 131:989–1002
109. Wachsstock DH, Schwartz WH, Pollard TD. 1993. Affinity of alpha-actinin for actin determines the structure and mechanical properties of actin filament gels. *Biophys. J.* 65:205–14
110. Wachsstock DH, Schwartz WH, Pollard TD. 1994. Crosslinker dynamics determine the mechanical properties of actin gels. *Biophys. J.* 66:801–9
111. Wang N, Butler JP, Ingber DE. 1993. Mechanotransduction across the cell surface and through the cytoskeleton. *Science* 260:1124–27
112. Xu J, Palmer A, Wirtz D. 1998. Rheology and microrheology of semiflexible polymer solutions: actin filament networks. *Macromolecules* 31:6486–92
113. Xu J, Tseng Y, Wirtz D. 2000. Strain-hardening of actin filament networks—regulation by the dynamic crosslinking protein α-actinin. *J. Biol. Chem.* 275:35886–92
114. Xu J, Viasnoff V, Wirtz D. 1998. Compliance of actin filament networks measured by particle-tracking microrheology and diffusing wave spectroscopy. *Rheol. Acta* 37:387–98
115. Xu J, Wirtz D, Pollard TD. 1998. Dynamic cross-linking by alpha-actinin determines the mechanical properties of actin filament networks. *J. Biol. Chem.* 273:9570–76
116. Yamada S, Wirtz D, Kuo SC. 2000. Mechanics of living cells measured by laser tracking microrheology. *Biophys. J.* 78:1736–47
117. Zhou X, Rowe RG, Hiraoka N, George JP, Wirtz D, et al. 2008. Fibronectin fibrillogenesis regulates three-dimensional neovessel formation. *Genes Dev.* 22:1231–43

Annu. Rev. Biophys. 2009.38:301-326. Downloaded from arjournals.annualreviews.org
by University of California - Berkeley on 04/07/10. For personal use only.

Annual Review of Biophysics
Volume 38, 2009

Contents

Frontispiece
Sunney I. Chan xii

A Physical Chemist's Expedition to Explore the World of Membrane Proteins
Sunney I. Chan 1

Crystallizing Membrane Proteins for Structure Determination: Use of Lipidic Mesophases
Martin Caffrey 29

Advances in Imaging Secondary Ion Mass Spectrometry for Biological Samples
Steven G. Boxer, Mary L. Kraft, and Peter K. Weber 53

Controlling Proteins Through Molecular Springs
Giovanni Zocchi 75

Electron Crystallography as a Technique to Study the Structure on Membrane Proteins in a Lipidic Environment
Stefan Raunser and Thomas Walz 89

Nuclear Envelope Formation: Mind the Gaps
Banafshé Larijani and Dominic L. Poccia 107

The Interplay of Catalysis and Toxicity by Amyloid Intermediates on Lipid Bilayers: Insights from Type II Diabetes
James A. Hebda and Andrew D. Miranker 125

Advances in High-Pressure Biophysics: Status and Prospects of Macromolecular Crystallography
Roger Fourme, Eric Girard, Richard Kahn, Anne-Claire Dhaussy, and Isabella Ascone 153

Imaging Transcription in Living Cells
Xavier Darzacq, Jie Yao, Daniel R. Larson, Sébastien Z. Causse, Lana Bosanac, Valeria de Turris, Vera M. Ruda, Timothee Lionnet, Daniel Zenklusen, Benjamin Guglielmi, Robert Tjian, and Robert H. Singer 173

Annu. Rev. Biophys. 2009.38:301-326. Downloaded from arjournals.annualreviews.org
by University of California - Berkeley on 04/07/10. For personal use only.

A Complex Assembly Landscape for the 30S Ribosomal Subunit
Michael T. Sykes and James R. Williamson 197

Mechanical Signaling in Networks of Motor and Cytoskeletal Proteins
Jonathon Howard 217

Biochemical and Structural Properties of the Integrin-Associated Cytoskeletal Protein Talin
David R. Critchley 235

Single-Molecule Approaches to Stochastic Gene Expression
Arjun Raj and Alexander van Oudenaarden 255

Comparative Enzymology and Structural Biology of RNA Self-Cleavage
Martha J. Fedor 271

Particle-Tracking Microrheology of Living Cells: Principles and Applications
Denis Wirtz 301

Bioimage Informatics for Experimental Biology
Jason R. Swedlow, Ilya G. Goldberg, Kevin W. Eliceiri, and the OME Consortium 327

Site-Directed Spectroscopic Probes of Actomyosin Structural Dynamics
David D. Thomas, David Kast, and Vicci L. Korman 347

Lessons from Structural Genomics
Thomas C. Terwilliger, David Stuart, and Shigeyuki Yokoyama 371

Structure and Dynamics of Membrane Proteins by Magic Angle Spinning Solid-State NMR
Ann McDermott 385

Index

Cumulative Index of Contributing Authors, Volumes 34–38 405

Errata

An online log of corrections to *Annual Review of Biophysics* articles may be found at http://biophys.annualreviews.org/errata.shtml

Annu. Rev. Biophys. 2009.38:301-326. Downloaded from arjournals.annualreviews.org
by University of California - Berkeley on 04/07/10. For personal use only.